Ocean and Coastal Research

Original Article
Special Article Collection
Braga, E. S.; Azevedo, J.S.; Harari, J.; Castro, C. G. (Eds.), Research in a RAMSAR site: The Cananéia-Iguape-Peruibe estuarine-lagoon complex, Brazil
http://doi.org/10.1590/2675-2824071.22075bos
ISSN 2675-2824

Sinking particles in the photic zone: relations with biogeochemical properties in different sectors of the Cananéia-Iguape Estuarine-Lagoon Complex (CIELC)-Brazil

Bruno, O. Sutti[1*], Vitor, G. Chiozzini[1], Carmen, G. Castro[2], Elisabete, S. Braga[1]

[1] Laboratory of Biogeochemistry of Nutrients, Micronutrients and Traces in Oceans – LABNUT-IOUSP Institute of Oceanography - University of São Paulo. Praça do Oceanográfico 191.05508-120São Paulo, SP, Brazil.
[2] Instituto de Investigaciones Marinas C/Eduardo Cabello, 6 – Vigo Pontevedra, Spain.

* Corresponding author: brunoosutti@gmail.com

Abstract

Over the last decades, regional climate changes, erosion, and heightened agricultural runoffs have increased nutrient and particle input in rivers, unbalancing the biogeochemical cycle of this suspended material along estuaries. In this context, particle fluxes in the euphotic zone, a very productive layer and important to maintain the food chain and estuarine preservation, require better understanding. This study aims to evaluate particle sedimentation fluxes in the photic zone of the Cananéia-Iguape Estuarine-Lagoon Complex (CIELC), considering sectors under different salinities and trophic statuses. A cylindrical sediment trap was installed at the base of the photic layer to measure particle fluxes and photopigments. Meanwhile, water samples were taken to measure temperature, salinity, pH, dissolved oxygen, and nutrients. Valo Grande (a freshwater domain) showed high nutrient concentrations, in which high fluxes of phaeopigments and chlorophyll-b highlighted the contribution of vegetable detritus to particle sinking. In the Batatais mangrove creek, the high fluxes of organic particles (675.32 mg m^{-2} d^{-1}) and chlorophyll-a (98.40 mg m^{-2} d^{-1}) evinced a high contribution of microplankton to carbon sinking. During the winter of 2018, flocculation processes were evinced in the flood tide of the Cananéia Bay as an important driver of sedimentation rates, with considerable fluxes of inorganic particles (1161.20 mg m^{-2} d^{-1}) and chlorophyll-a (83.27 mg m^{-2} d^{-1}). In the summer of 2019, we observed a lower flux in total particles (451.24 mg m^{-2} d^{-1}) in a period of haline stratification. In the Ararapira Channel, the lowest organic particle fluxes (<100 mg m^{-2} d^{-1}) were associated with ultra-oligotrophic conditions, indicating a low influence of microplankton on sinking particles. These findings suggest that freshwater input, tidal variation, and trophic status are relevant controls of sinking particles in different CIELC sectors.

Keywords: Sinking particles, Subtropical estuary, Trophic status, Photosynthetic pigments, Anthropogenic influence

Submitted: 13-Jun-2022
Approved: 05-Jun-2023
Editor: Rubens Lopes
Associate Editor: Juliana Azevedo

INTRODUCTION

Among coastal environments around the world, estuaries show the most relevant ecosystems concerning carbon storage while being the most pressured by human activities. Moreover, these aquatic systems are the most significant concerning the exchange of suspended material between the continent and adjacent seas. Suspended material (including dissolved/particulate and organic/inorganic forms) undergoes intense physical and biogeochemical modification during its transport along the river-ocean continuum. These modifications are induced by natural processes and anthropogenic interferences, which can configure significant pathways in the carbon cycle. Thus, the biogeochemistry of suspended material in estuaries (focusing on the carbon cycle and its relation to environmental conditions) is an essential theoretical approach to better understand the human influence on climate change, as well as the ways to mitigate it.

Mangrove and tidal marsh ecosystems sequester and store carbon when they are protected or restored and emit greenhouse gases when degraded or destroyed (Beltran et al., 2012; Saderne et al., 2019). Meanwhile, adjacent estuarine bodies of water have been estimated as CO_2 emitters due to the organic production of these wetland ecosystems and the increasing anthropogenic inputs into rivers over the last 200 years (Cole et al., 2007; Regnier et al., 2013). Therefore, it is essential to consider the biogeochemical differences that occur among estuarine zones, especially between mangrove creeks and estuarine areas (such as channels and lagoons) since they display distinct sedimentation rate (Kathiresan, 2003), nutrient availability, and plankton composition dynamics (Tundisi and Matsumura-Tundisi, 2001; Kathiresan, 2003; Cotovicz Junior et al., 2012; Choudhury and Bhadury, 2015; Santos et al., 2021).

In the euphotic zone, nutrients are used during photosynthesis to generate particulate and dissolved contents that sink or are mixed during their transport along aquatic systems. Marine phytoplankton plays a critical role in the global carbon cycle via the biological carbon pump, which is the biologically driven sequestration of carbon by the ocean from the atmosphere to seafloor sediments (Emerson and Hedges, 2008; Karlusich et al., 2020). The biological carbon pump depends on four main pools (dissolved inorganic carbon, dissolved organic carbon, particulate inorganic carbon, and particulate organic carbon [POC]), which are interlinked by a series of key processes beyond primary production, such as grazing, secondary production, respiration, excretion, aggregation, calcification, and others (Brewin et al., 2021). This study is the first to measure the sedimentation rates of particles in Brazilian estuaries by a sediment trap developed in the photic zone, investigating their relations with dissolved nutrients (inorganic and organic forms) and proportions between particulate inorganic matter (PIM) and particulate organic matter (POM). Owing to the high productivity and large concentration of suspended mineral matter, sediment traps deployed in adjacent seas and estuarine areas can collect a large number of particles in a short time (Zajączkowski, 2002; Froján et al., 2016; Zuñiga et al., 2016).

Among the eutrophication effects on aquatic ecosystems, it is important to consider the increased growth of macroalgae, phytoplankton blooms, changes in plankton composition, oxygen depletion, and increased sedimentation rates as events highly related to the organic matter dynamic (Chislock et al., 2013; Hao et al., 2021). In parallel to nutrient analysis in the water column, the identification of photosynthetic pigment composition has been an important tool for verifying the ecological features (related to cell size and physiological conditions) of the predominant phytoplankton groups in subtropical/tropical estuaries (Chai et al., 2016; Damar et al., 2020). Moreover, trophic state indexes have been widely used to evaluate eutrophication levels in coastal environments (Primpas and Karydis, 2010; Cotovicz Junior et al., 2012; Santos et al., 2021), whereas the N:P:Si ratio has been an essential parameter to better understand the impacts of climate changes (regarding the increase of extreme

precipitations) on coastal eutrophication (Billen and Garnier, 2007; Garnier et al., 2010; Raimonet et al., 2018).

Sedimentation rates in estuaries can display high spatiotemporal variability, depending on the physical and biogeochemical properties of particles (i.e., shape, gravity, density, lability, types of chemical bonds, and microbiodiversity) and the environmental conditions to which they are exposed, such as wind forcing, solar radiation, water circulation pattern, turbulence, transparency, salinity, pH, redox potential, and temperature. Estuarine circulation (driven by tidal range and river flow) promotes a spatiotemporal variation in salinity, thereby establishing sites with distinct levels of particle trapping (Bianchi, 2006) and, consequently, distinct carbon dynamics in the atmosphere-water-sediment interfaces (Joesoef et al., 2015; Rassmann et al., 2016). The effect of variations in salinity on flocculation processes, which has been shown for clay particle aggregation (Thill et al., 2001; Mari et al., 2012), is a key issue in studies that assess carbon sinking in estuaries. The speed of this process, in turn, can be strongly enhanced by diatom blooms (Pilskaln et al., 1996; Verney et al., 2009; Kostadinov et al., 2012; Zhang et al., 2014).

Based on this context, this study aims to evaluate the sedimentation rates of particles in the photic zone and their relations with the physical and biogeochemical properties (such as salinity, pH, dissolved nutrients, N:P:Si ratios, and a trophic state index) of estuarine sectors with varying geomorphology, hydrodynamic, and anthropogenic interventions.

METHODS

Study area

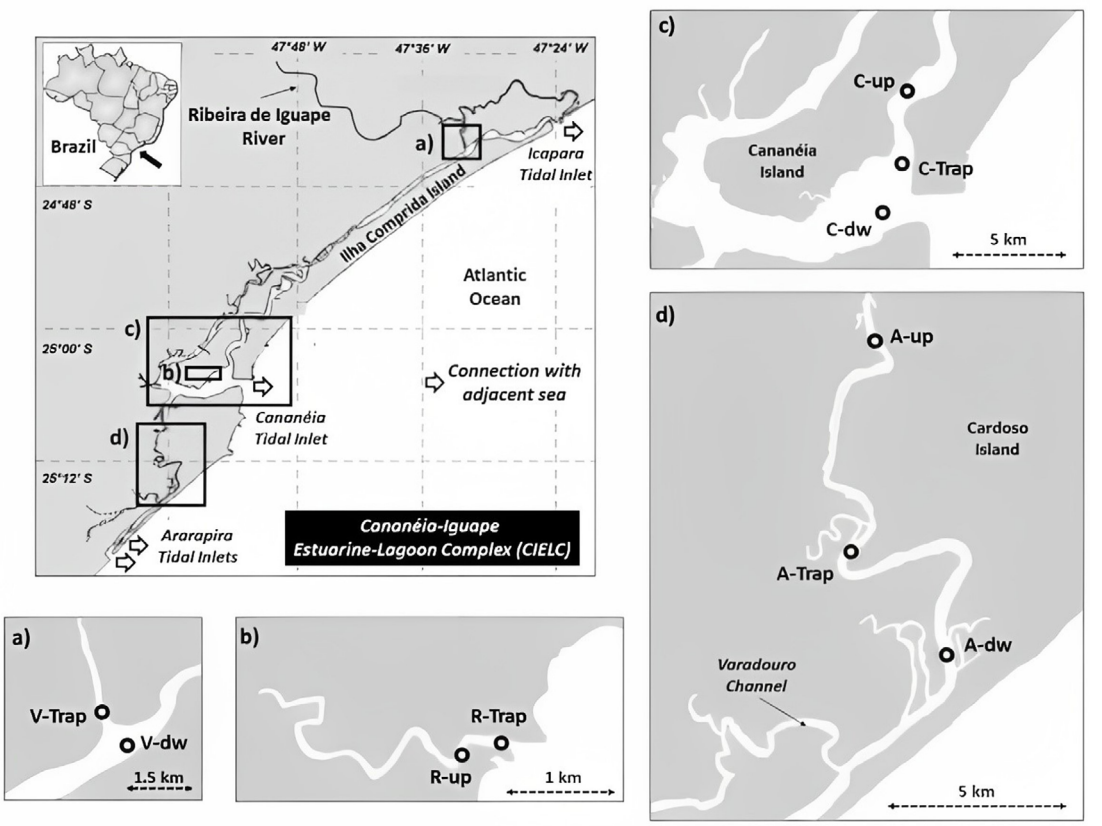

Figure 1. Map of the Cananéia-Iguape Estuarine-Lagoon Complex (CIELC), highlighting its estuarine sectors (Google Earth Pro, 2017) and their respective sampling stations: a) the Valo Grande Channel (V stations); b) the Batatais mangrove creek (R stations); c) the Cananéia Bay (C stations); and d) the Ararapira Channel (A stations). Note: up and dw = secondary stations located upstream and downstream from the trap stations, respectively.

The Cananéia-Iguape Estuarine-Lagoon Complex (CIELC) (Figure 1) is included in the list of wetlands of international importance (RAMSAR, 2017). This estuarine region comprises the largest remnants of the Atlantic Rainforest in South America, along with mangrove and *restinga* forests and bays that support large numbers of species (UNESCO, 1999). The São Paulo coast is influenced by a microtidal regime (Miyao et al., 1986; Arasaki and Alfredini, 2009) and has a wet tropical climate with a rainfall index often exceeding 200 mm in the summer (December–March) (Silva, 1989; Nunes, 1990).

The northern and southern regions of the CIELC show considerable differences regarding their geomorphological features, freshwater influence, and anthropogenic pressure. Iguape City, in the northern area (50,000 inhabitants), sits on the banks of the Ribeira River, in which mining, agriculture, and fishing have been historically important economic activities. To facilitate the exportation of these products by ship, an artificial channel (Valo Grande) linking the Ribeira River to the lower estuary was inaugurated in 1852. The Valo Grande channel was closed with a dam and reopened twice between 1978 and 1995, when it was finally left open (Prado et al., 2019). As a result of freshwater input via the Valo Grande (Figure 1a), the salinity of the northern section was considerably reduced, and great river discharges during summertime (February–March) started to modify the water circulation (e.g., increasing water column stratification) in the southern sectors (Cubatão and Cananéia channels) (Arasaki and Alfredini, 2009).

The lower region of the Cananéia channel (Cananéia Bay) is located in a large coastal plain highly influenced by coastal processes (conditioned by the Cananéia tidal inlet dynamic). Thus, this region constitutes an estuarine-lagoon complex (Trapandé and Cananéia bays) (Figure 1c) in which sedimentary formation is less represented by fluvial sediments and more represented by lagoon (sand and clay) and coastal marine sediments (sands) (Giannini et al., 2009). In this estuarine sector, the primary driving mechanisms are the longitudinal salinity gradient and freshwater discharge (Miranda and Castro Filho, 1996). Due to their origin in plain insular areas (the Cananéia and Ilha Comprida islands), the tributary rivers of the Cananéia Bay are small and have low discharge, thus acting as tidal creek systems in the mangrove and *restinga* areas (Figure 1b).

In addition to the Mar Pequeno estuarine channel (in the northern region) and the estuarine-lagoon complex (Trapandé, Cubatão, and Cananéia bays), the Ararapira estuarine channel is considered another large estuarine sector with its own particular geomorphological and hydrodynamic signatures. Differing from classical estuary models, the Ararapira Channel has inlets connecting the estuary to the adjacent sea and other estuarine sectors (Trapandé Bay and the Varadouro Canal) (Angulo et al., 2019), thereby providing a tidal-wave convergence in its central region (from the Trapandé Bay to the mouth of the Varadouro Canal) (Figure 1d). We should also mention the multiple riverine inputs (from mountain ranges on both the continent and Cardoso Island) in the northern region and a recent (August 20, 2018) morphodynamic phenomenon (barrier-inlet systems) that established a new tidal inlet in the southern region (Italiani et al., 2020).

Sampling strategy and sediment trap use

Valo Grande (freshwater domain), the Cananéia Bay (estuarine lagoon), the Batatais River (internal mangrove creek), and the Ararapira Channel (estuarine channel) were the CIELC estuarine sectors chosen to install the sediment trap. Sinking particles and their relations with physical and biogeochemical properties were studied using data obtained at the beginning (B) and end (E) of the sediment trap exposure to the water column. At least one additional station (near the Trap station) was also defined for each estuarine sector to collect water samples (Figure 1). In the Valo Grande sector (V), the additional station was placed downstream (V-dw) from the V-Trap, whereas in the Batatais Creek sector (R), it was placed upstream (R-up) from the R-Trap. In the case of the Cananéia Bay (C) and Ararapira Channel (A) sectors, the additional stations were defined both upstream (C-up and A-up, respectively) and

downstream (C-dw and A-dw, respectively) from the C-Trap and A-Trap stations, respectively.

In the winter of 2018, sectors V and R were sampled on July 3-5 and the C and A sectors, on August 22–23. In the summer of 2019, sampling was performed on February 13–14 in the A and C sectors. Meteorological data were obtained from an official station (INMET, 2020) near the Valo Grande Channel, whereas tidal heights were recorded using a tide gauge located in the lower zone of the Cananéia Bay (IO-USP, 2006).

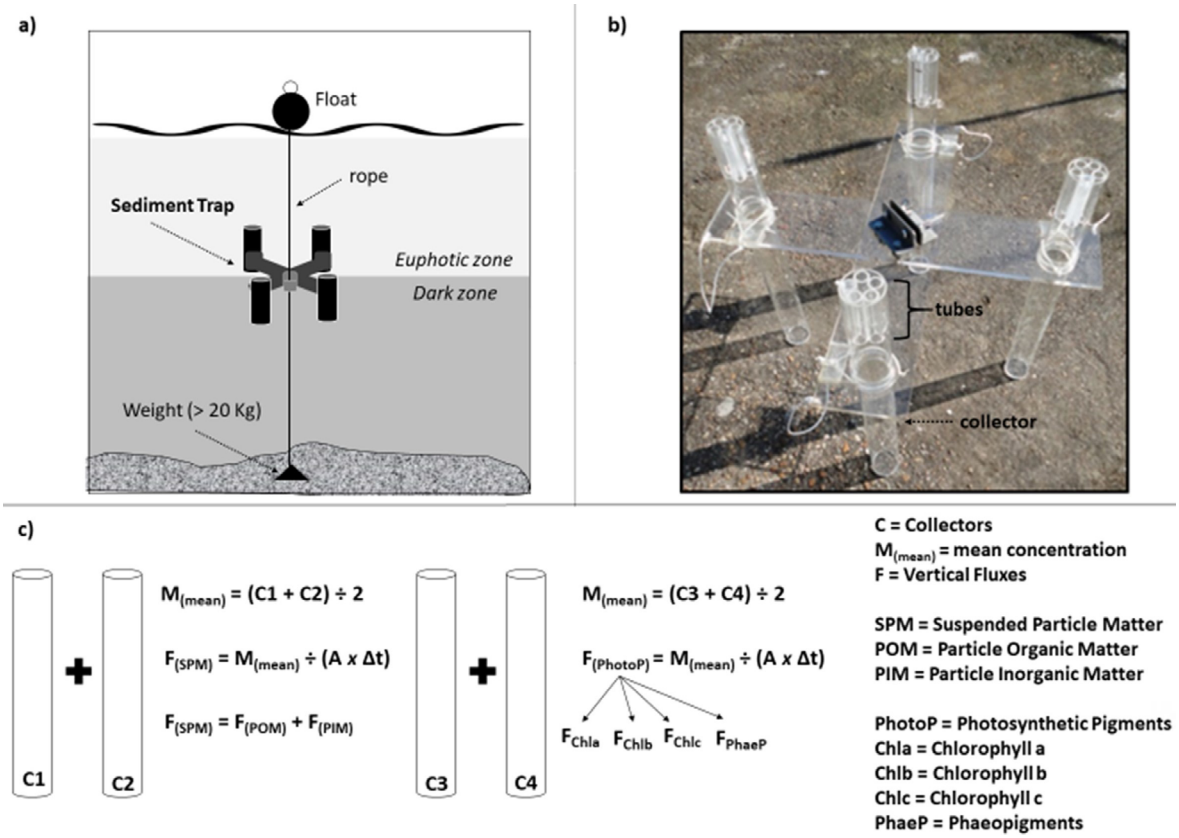

Figure 2. a) Operation mode of the sediment trap in the water column, specifying its accessory materials; b) cylindrical sediment trap structure built at LABNUT-IOUSP following Dr. Carmen Castro' project; and c) method adopted to measure particle sedimentation rates: two collectors (C1 and C2) were used to estimate the vertical fluxes of suspended particle matter (FSPM) and the other two (C3 and C4), the vertical fluxes of particles related to photosynthetic pigments (FPhotoP).

Onboard the Albacora research vessel (Oceanographic Institute of the University of São Paulo - IO-USP), the local and photic zone depths were measured using sonar and a Secchi disk (Sd), respectively. The accessory materials of the sediment trap were adjusted according to the local and Sd depths to place the sediment trap at the base of the photic zone (Figure 2a). Water samples had been previously collected to quickly determine their salinity using an RTS-101ATC (Instrutherm®) refractometer. This was done to fill the trap collectors with a saline solution (an NaCl solution 5 psu above the local salinity). This procedure prevents the collected water from being exchanged with outside waters (Froján et al., 2016). The sediment trap consisted of four acrylic cylindrical collectors with a height of 60 cm and diameter of 6 cm (Figure 2a). To minimize the loss of the collected material as a result of turbulence, each collector had an internal structure (six small plastic tubes) fixed to the upper portion of the trap (Figure 2b), as recommended by Dr. Carmen

Castro (Institute of Marine Research - ESP) for coastal waters. The collector tube dimensions and substructures of the sediment trap used in this study were evaluated as the best adaptation for cylindrical sediment traps to minimize losses due to turbulence in aquatic systems (Buesseler et al., 2007).

The suspended particulate matter (SPM) (including photosynthetic pigments – PhotP) was retained in the cylinder traps over a 1.5-6.5-hr exposure time at each selected point. The water was filtered using Whatman® GF/F membranes (47 mm Ø; 0.45 µm) — which were previously weighed and combusted at 450 °C for 4h30 following the gravimetric method described by Strickland & Parsons (1968) — to determine SPM and its organic fraction (POM). After filtration, the membranes were stored at –20ºC until laboratory analysis. Once their masses were determined (Figure. 2c), vertical fluxes (FSPM and FPhotP) were calculated as follows:

$$F = M/(A * \Delta T)$$

in which

M represents the mean masses (estimated using the content of two collectors) of the particulate matter and PhotP (mass extracted from SPM and used to determine the fluxes);

A represents the area (cylinder) of the sediment trap collector, and

ΔT (h) represents the exposure length (interval) of the Trap in the water column.

The water column was sampled at the beginning (B) and end (E) of the sediment trap exposure to record its temperature, salinity, pH, dissolved oxygen [DO], and nutrients (Si, N, and P). The same measurements were conducted at the additional stations. Each water sampling period provides data from the photic (surface layer) and aphotic (bottom layer) zones, except at the V-trap station, which provided data from only one layer (1.2 m). Water temperature was measured using a protected reversing mercury thermometer coupled to Hydrobios® bottles, which were used to collect water samples for DO, pH, and ammonium analysis. Moreover, van Dorn bottles were used to collect water samples for the other analyses.

Immediately after sampling, DO was determined according to the Winkler method (Grasshoff et al., 1983), using a Metrohm® burette, whereas pH was measured using an Orion® pH-meter with a precision of 0.001. Dissolved oxygen saturation (DO%) was calculated using the equations proposed in Aminot and Chaussepied (1983). The filters were defrosted in a laboratory for SPM and PhotP analysis. SPM and organic (POM) and inorganic (PIM) fractions were determined according to Strickland and Parson (1968). Chlorophylls (a, b, and c) and phaeopigments (PhaeP) were analyzed by spectrophotometric methods following Jeffrey and Humphrey (1975) and Lorenzen (1965), respectively.

Analysis of dissolved nutrients

Dissolved nutrients were analyzed by colorimetric methods. The determination of dissolved silicate (DSi) and dissolved inorganic phosphorus (DIP) followed the methods described in Grasshoff et al. (1983) with precisions of 0.02 and 0.01 µmol L^{-1}, respectively. Under precisions of 0.01 µmol L^{-1}, ammonium ($N\text{-}NH_4^+$) was determined following the method described by Tréguer and Le Corre (1975), whereas nitrate ($N\text{-}NO_3^-$) and nitrite ($N\text{-}NO_2^-$) were measured using an Auto-Analyzer II (BranLuebbe®), following the methods described by Tréguer and Le Corre (1975) and Grasshoff et al. (1983), respectively. Dissolved inorganic nitrogen (DIN) was calculated as the sum of $NH4^+$, NO^-, and $NO3^-$. Urea content was determined using the analysis described by Aminot and Kerouel (1983). The detection limit of the method was 0.01 µmol L^{-1} of N-Urea. Dissolved organic nitrogen (DON) and dissolved organic phosphorus (DOP) levels were analyzed using UV-oxidation, describing total dissolved nitrogen (TDN) and phosphorus (TDP) contents based on Armstrong et al. (1966) and following the recommendations in Braga (2020), using the appropriate equipment (patented by the Laboratory of the Biogeochemistry of Nutrients, Macronutrients, and Traces in the ocean at the Oceanographic Institute, University of São Paulo) based on a potent UV lamp (1,300W–2,000-2,500Å).

Trophic Status Equation (TRIX) and Statistics Analysis

This study adopted the TRIX equation proposed by Vollenweider et al. (1998) as follows:

$$TRIX = [\log (DIP * DIN * Chla * dDo\%) + a]/b$$

In which

dDO% is the absolute deviation of dissolved oxygen saturation and a (1.5) and b (1.2) are scale coefficients.

The a and b coefficients were proposed by Giovanardi and Vollenweider (2004) to fix the scale range from 0 to 10. Primpas and Karydis (2010), when assessing the TRIX in oligotrophic marine environments, questioned the universal use of this index and suggested that the scaling of TRIX should be specific to a region. The TRIX scale (Table 1), which has been adopted for Brazilian coastal environments (Cotovicz Junior et al., 2012; Santos et al., 2021), was used in this study.

Descriptive and multivariate statistics were performed in GraphPad Prism®. The concentrations of pigments (Chla + Chlb + Chlc + PhaeP), nutrients (DSi + DIN + DON + DIP + DOP), and nitrogen forms (nitrate + nitrite + ammonium + urea) are expressed in stacked bar charts. The Shapiro–Wilk test was used to test the normality of column water data. Finally, Pearson correlation (N = 42) and principal component analysis (PCA) were conducted to verify the physical and biogeochemical relationships between the dissolved and particulate forms observed in the water column and then their association level with sinking particles.

Table 1. Classification of trophic status for estuarine waters according to the trophic index (TRIX) model.

TRIX	Conditions	Trophic State
<2	Very poorly productive water and very low trophic status	Excellent (Ultra-Oligotrophic)
2-4	Poorly productive water and low trophic status	High (Oligotrophic)
4-5	Moderately productive water and medium trophic status	Good (Mesotrophic)
5-6	Moderate to very productive water and high trophic status	Moderate (Meso to Eutrophic)
6-8	Very productive water and high trophic status	Poor (Eutrophic)
8-10	Highly productive water and highest trophic status	Very Poor (Hypereutrophic)

RESULTS AND DISCUSSION

Weather conditions and tide ranges during sediment trap exposure

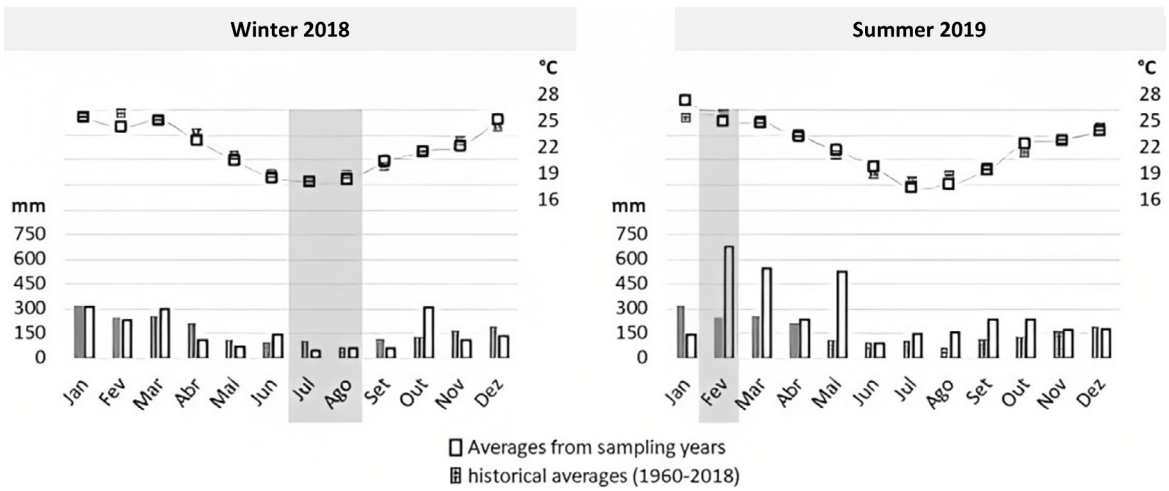

Figure 3. Monthly average temperature (squares) and accumulated rainfall (histograms) values (CIIAGRO, 2020). Shaded areas correspond to the months of sampling.

In July and August 2018, average air temperature and accumulated rainfall reached values similar to the historical data for the region (Figure 3), i.e., data were typical for dry winter months in which rainfall normally fails to exceed 150 mm. February 2019 also showed an average air temperature similar to the historical average, but accumulated rainfall was considerably higher. At the latitudes of the São Paulo coast (23°22'-23°19' S), increases in the frequency and intensity of extreme weather events in recent decades have contributed to positive trends in total seasonal and average daily precipitation. On this coast, the higher volumes of daily precipitation (over the last 70 years), mainly in the summer months, are related to the intensification of precipitation rates due to the increase (by about 1 °C) in the surface temperature of the Atlantic Ocean (off the coast of São Paulo) (Zilli et al., 2016). The low rainfall volumes reported before sampling days (July and August) indicated that the CIELC was influenced by two periods of low river discharges. In contrast, note that the sampling days in February 2019 fell within a period of heavy rainfall (Figure 4), which probably resulted in considerable river discharges.

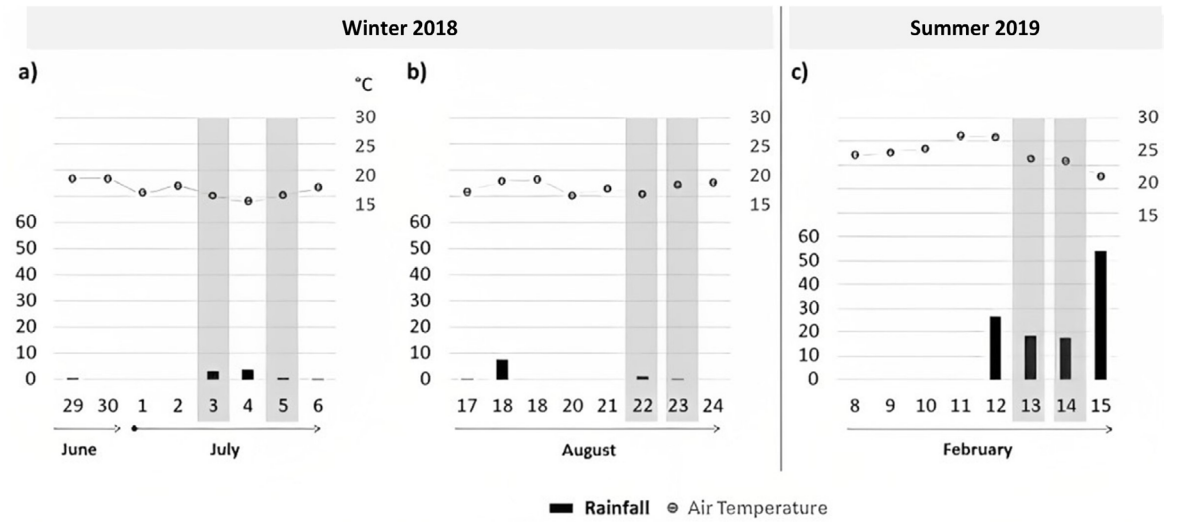

Figure 4. Daily air temperature (average) and rainfall (accumulated) relative to a period of 4-6 days before the sampling day (INMET, 2019). Shaded areas correspond to the following sampling days: a) V (July 03), b) R (July 05), c) C (August 23), d) A (August 22), e) C (February 14), and f) A (February 14).

Figure 5 shows the exposure time of the sediment trap within the tidal range in each estuarine sector. Based on the average maximum limit (1.2 m) of the regional microtidal height (Arasaki and Alfredini, 2009), CIELC was driven by spring tides during the sampling periods in winter 2018 and by neap tides during the sampling periods in summer 2019. According to the tidal curves relative to the sampling days of winter 2018, the sediment trap was set during flood tides in sectors V (Figure 5a) and C (Figure 5c), during the beginning of the ebb phase in Sector R (Figure 5b), and during the high tide and a part of the ebb phase in Sector A (Figure 5d). In summer 2019, the sediment trap was installed during the high tide in Sector C (Figure 5e) and during the ebb phase and part of the subsequent flood phase in Sector A (Figure 5f).

Figure 6 shows the variation in radiation during the period in which the sediment trap was exposed at the base of the photic zone in the four estuarine sectors. In winter 2018, Sector V showed values between 180 and 250 KJ m^{-2} (Figure 6a), whereas Sector R was under null radiation from 10:00 to 11:00, with an exponential increase from 11:00 to 11:30 (up to 400 KJ m^{-2}) (Figure 6b). In turn, Sector C was under null radiation from 07:35 to 10:00, with an exponential increase from 10:00 to 12:50 (up to 800 KJ m^{-2}) (Figure 6c). Finally, Sector A was

under low radiation (70 KJ m^{-2}) at the beginning of the trap exposure time (11:38) and under higher intensities for most of the trap exposure time (13:00–17:20), ranging from 300 to 800 KJ m^{-2} (Figure 6 d). In the summer of 2019, the sediment trap in Sector C was under null radiation from 8:00 to 10:00, with an exponential increase from 10:00 to 12:00 (up to 1630 KJ m^{-2}) (Figure 6e), whereas, in Sector A, the trap was under increasing radiation (0-985 KJ m^{-2}) from the beginning (8:15) to the end (12:15) of its exposure time.

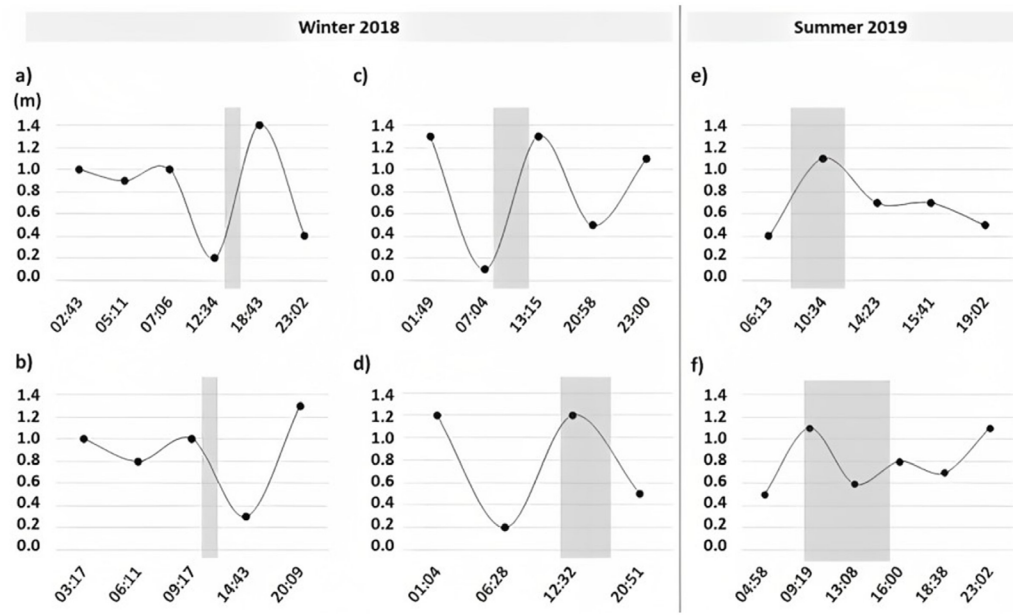

Figure 5. Tidal curves relative to sampling days. Shaded areas highlight the exposure time of the trap in each station: a) V (July 03), b) R (July 05), c) C (August 23), d) A (August 22), e) C (February 14), and f) A (February 14).

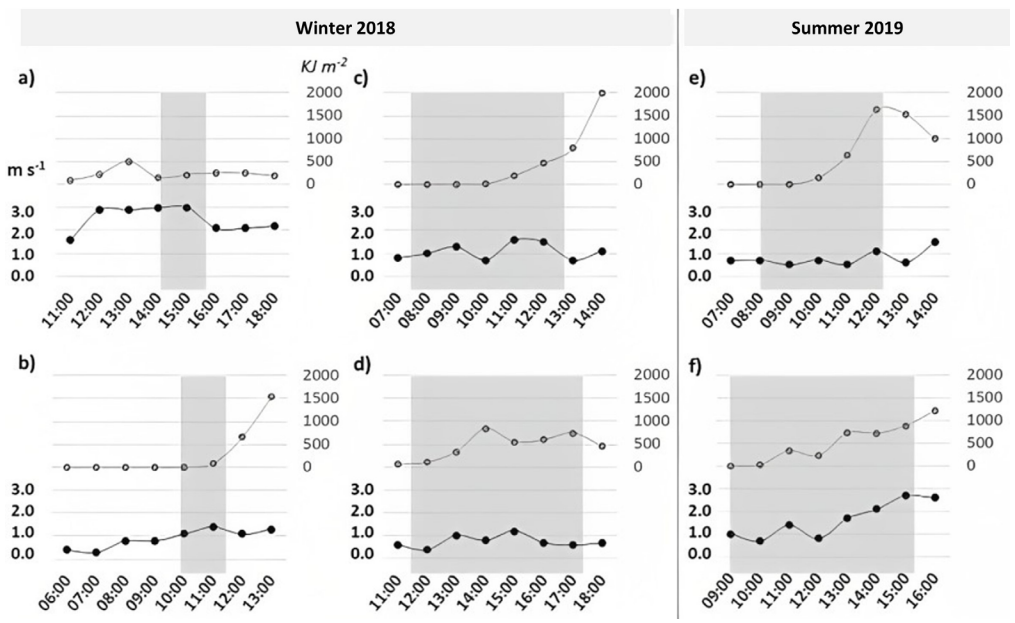

Figure 6. Surface wind speed (ms^{-1}) and solar radiation (KJ m^{-2}) per hour (INMET, 2019). The highlighting in shaded areas indicates the exposure time of the trap in each station: a) V (July 03), b) R (July 05), c) C (August 23), d) A (August 22), e) C (February 14), and f) A (February 14).

In winter 2018, southerly winds (< 3.0 m s^{-1}) and low solar radiation (< 800 KJ m^{-2}) (INMET, 2020) predominated during the sampling period. These atmospheric conditions, which are associated with air temperatures ranging from 16 to 20 °C and high cloud cover (Table 2), are typical of winter periods under a cold front. On the São Paulo coast, this weather front leads to a wind that rotates from east to north and west and an atmospheric pressure fall of about 10 hPa, followed by southerly winds (between 3 and 10 m s^{-1}) and air temperatures decreasing by about 5 °C (Harari et al., 2008).

Table 2 shows the MetOcean variables reported at the beginning (B) and end (E) of the sediment trap exposure at the base of the photic zone in the four estuarine sectors. Cloud cover and radiation along the trap exposure varied considerably; whereas Secchi disk depths (SD) showed slight differences between B and E times, suggesting that the photic zone height showed low variation during trap exposure in the estuarine sectors. The differences in local depths (LD) between B and E times responded to tidal ranges, reaching maximum amplitudes in the C-Trap station in both winter and summer (Table 2).

Table 2. MetOcean parameters reported at the beginning (B) and end (E) of the sediment trap exposure to the water column and concentrations of suspended particulate matter (SPM) at the bottom (*) and surface (**) layers. Note: SD (Secchi depth); LD (local depth); BL (sampling bottom layer); and TD (operation depth of the sediment trap above the bed). TD was estimated by subtracting SD from LD.

Trap Stations	Exposure Time		Cloud Cover	Radiation (KJ m-2)	SD (m)	LD (m)	TD (m)	BL (m)	SPM (mg L-1)	
Winter 2018									(*)	(**)
(V)	**B**	14:45	8/8	180	1.2	4.3	3.1	1.2	10.71	8.87
	E	15:45	8/8	250	1.2	4.5	3.3	1.2	7.72	10.38
(R)	**B**	10:00	8/8	0	1.0	3.8	2.8	3.0	36.71	39.57
	E	11:30	6/8	400	1.2	4.5	3.2	3.0	35.86	33.57
(C)	**B**	7:35	8/8	0	1.5	6.0	4.5	5.0	88.68	35.74
	E	12:50	5/8	800	1.5	6.8	5.3	5.0	68.94	50.91
(A)	**B**	11:38	8/8	70	4.1	5.7	1.6	3.0	88.57	29.25
	E	17:23	7/8	800	4.0	5.0	1.0	3.0	42.33	40.00
Summer 2019										
(C)	**B**	8:15	8/8	0	1.5	6.0	4.5	5.0	45.33	34.17
	E	12:12	6/8	1630	1.5	6.8	5.3	5.0	46.00	33.50
(A)	**B**	9:10	8/8	0	1.5	5.8	4.3	5.0	49.67	25.00
	E	15:26	7/8	1100	1.2	5.8	4.6	5.0	55.93	43.33

Possible sampling biases of the sediment trap regarding hydrodynamic issues

Sediment traps have several possible sampling biases, such as those due to hydrodynamic issues, swimmer effects, and sample solubilization (Buesseler et al., 2007), of which the hydrodynamic issue is the most important because it is caused by the horizontal flow over the mouth of the trap, which may lead to under- or oversampling of sinking particulate materials (Baker et al., 1988; Gardner et al., 1997; Buesseler et al., 2007). The influence of horizontal flux on sediment trap efficiency is even more important in tidal environments (Bale, 1998; Wang et al., 2015). Gardner et al. (1997) found that cylindrical sediment traps showed no significant over- or under-collection at current velocities equal to 1-22 cm s^{-1}, whereas Baker et al. (1988) found that trapping efficiency decreased at current speeds higher than 12 cm s^{-1}. In turn, the review of Buesseler et al. (2007) reported that the temporal

conditions defined by Gardner et al. (1997) were more poorly constrained than those in Baker et al. (1988). The speed limit of 12 cm s^{-1} has been adopted in estuaries as a horizontal flux reference to analyze sediment trap accuracy (Zajączkowski, 2002; Johannessen et al., 2005; Froján et al., 2016).

CIELCI water circulation patterns remain poorly understood and have been detailed at only a few sites of the lagoon region (Cananéia, Cubatão, and Trapandé bays). Miranda and Castro Filho (1996) recorded maximum currents of about 11 cm s^{-1} (bottom layers) within a complete tidal spring cycle in the lower zone of Cananéia Bay (next to the C-Trap station). At this same site, Miyao and Harari (1989) estimated the highest CIELC currents using analyses of tidal height and tidal current data. Based on these findings, we suggest that the sediment trap set at the C- and R-Trap stations showed low sedimentation rates concerning local horizontal fluxes, regardless of exposure period within the tidal cycle. Despite no current tidal dataset about the Ararapira channel, weaker currents have been evinced in its central region (surrounding the A-Trap station) due to tidal-wave confluence (Angulo et al., 2019). The mouth of the Valo Grande Channel (V-Trap station) is subject to high currents driven by Ribeira River discharges and is another estuarine area that lacks hydrodynamic data. To ensure low hydrodynamic conditions during V-Trap exposure, we set it during the flood phase of a spring tide, a hydrodynamic condition that attenuates river flow.

Table 2 shows the sediment trap distance from the bottom layer (TD) and the SPM concentrations of bottom and surface waters. Using an ADCP (acoustic Doppler current profiler), Wang et al. (2015) monitored current velocities (horizontal fluxes) and SPM concentrations at the bottom layer. From these parameters, they evaluated trap collection efficiency according to bottom shear stress. These authors developed a sediment trap one meter above the bed in strong tidal sectors in Luoyuan Bay-China (mean tide range of 4.98 m), observing significant overestimation during a spring tide with current speeds from 30 to 60 cm s^{-1}.

Conversely, CIELC is on a microtidal coast (maximum tidal height of 1.40 m). Moreover, this study refers to a sediment trap installed at the base of the photic layer, i.e., distant from the bottom. Based on these factors, the influence of bottom shear stress on the collected material was probably low. Despite that, some sampling periods showed a considerably higher SPM concentration at the bottom layer (relative to the surface layer) (Table 2). In winter 2018, the high SPM concentrations (68.9-88.7 mg L^{-1}) found at the bottom layer (BL) in the C-Trap station (Cananéia Bay) may have responded to re-suspended bottom sediments during the flooding of the spring tide. In this case, BL (5.0 m) was close to TD (4.5-5.3 m), although it maintained a certain distance from the bed during exposure (B-E) (Table 2). In winter 2018, the A-Trap station (Ararapira channel) also showed a high SPM concentration at BL (sampled above the TD). This would be strong evidence of the influence of sediment resuspension on the collected material. However, this central region of the Ararapira channel is subjected to weaker currents due to the proximity of tidal-wave convergence (Angulo et al., 2019).

Physical and chemical properties of the water column

Temperature, salinity, pH, and dissolved oxygen

The water temperature in winter 2018 ranged from 19.2 (A-Trap station) to 21.2 °C (V-Trap station) and from 27.0 (A-Trap station) to 28.2 °C (A-upstream station) in summer 2019. This is a typical range of temperature for estuarine waters in the São Paulo coast (Moser et al., 2005; Azevedo and Braga, 2011; Braga, 2020)

In the Valo Grande region (Sector V) (Figure 7a), salinity reached almost zero (0.01-0.04), reflecting the domain of the Ribeira de Iguape river flow. In the Batatais mangrove creek (Sector R) (Figure 7b), the salinity range (29.37-30.00) showed the highest marine influence. Compared to sectors C (Cananéia Bay) and A (Ararapira channel), sectors V and R showed a lower variability in their physical and chemical parameters, which were favored by the shorter distances of the sampling stations (Trap and additional stations) and smaller

sampling intervals (B and E). Moreover, sectors V and R are naturally subject to lower salinity ranges due to the annual Ribeira de Iguape river discharges (via the Valo Grande Channel) and the geographic confinement of the Batatais Creek (under low freshwater input), respectively.

In winter 2018, both the Cananéia Bay and Ararapira Channel showed salinity ranges (23.90-29.44 and 28.8-30.11, respectively) indicating a higher marine influence on those sectors during the exposure of the sediment trap. In the Cananéia Bay (C-Trap station), the sediment trap was exposed for a period (B-E) under considered salinity differences (Figure 7c) in both surface (23.90-28.64) and bottom layers (24.43-28.84). On the other hand, the salinity in the Ararapira channel (A-Trap) had a low range (29.85-29.78 in its surface layer; 30.11-29.87 in its bottom layer) during the exposure (B-E) of the sediment trap (Figure 7d). These estuarine sectors showed no salinity gradients and haline stratification during the sampling period (winter 2018). In contrast, freshwater inputs (as a result of greater rainfall volumes) drove the salinity gradient (from upstream to downstream) and saline stratification along these estuarine sectors in the summer of 2019 (Figures 7e and 7f).

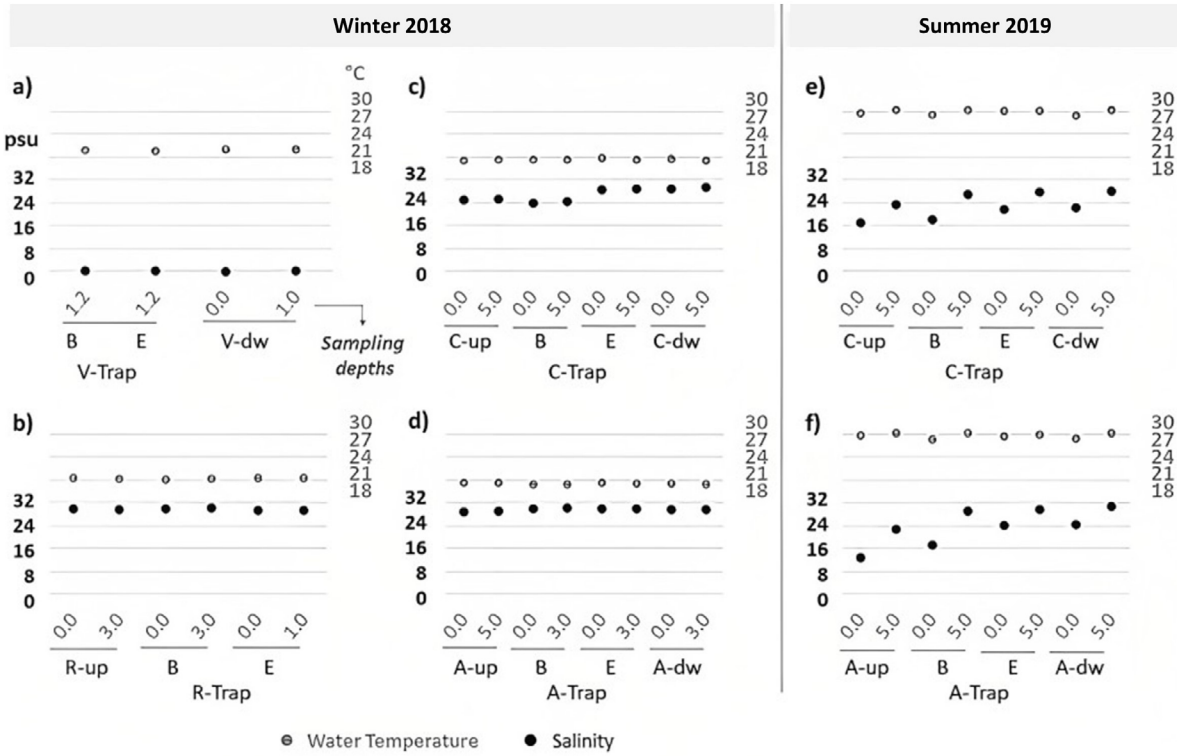

Figure 7. Temperature and salinity in the water column of the studied CIELC estuarine sectors: a) Valo Grande Channel (stations V); b) Batatais mangrove creek (stations R); c) and e) Cananéia Bay (stations C); and d) and f) Ararapira channel (stations A). Note: B and E (samples collected at the beginning and end of the sediment trap operation, respectively); up and dw (complementary stations located upstream and downstream from the Trap stations, respectively).

PH ranged from 7.57 (V-Trap station) to 8.05 (R-Trap station) (Figure 8). Generally, river waters display a lower pH than marine waters, and a linear increase in values occurs with salinity increases. It is important to take note that pH levels are influenced more strongly by salinity than by biological processes (Figures 7 and 8), which can be evinced by DO%. According to Breitburg (2002), hypoxic conditions in coastal waters are favored under DO% values below 50%. DO% ranged from 76.9 (A-Trap; summer 2019) to 102.3% (C- downstream; winter 2018), showing

good saturation in all four estuarine sectors. Moreover, we observed a slight decrease in DO% values from winter to summer in the Cananéia Bay and Ararapira Channel. Trap stations showed negligible differences in this parameter between sampling intervals (B–E), except in the A-Trap station (summer 2019), which had a surface layer DO% of 76.9% at the beginning and of 89.1% at the end of the exposure of the sediment trap to the photic zone.

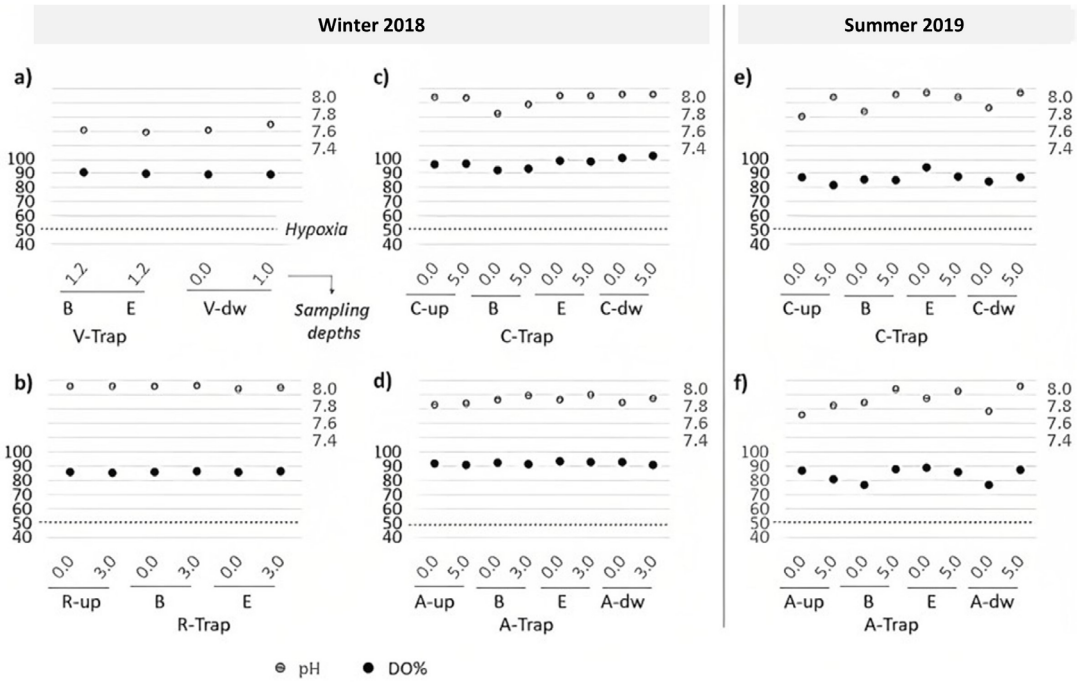

Figura 8. PH and oxygen saturation (DO%) in the water column of the estuarine sectors studied in the CIELC: a) Valo Grande Channel (stations V); b) Batatais mangrove creek (stations R); c) and e) Cananéia Bay (stations C); and d) and f) Ararapira channel (stations A). Note: B and E (samples collected at the beginning and end of the sediment trap operation, respectively); up and dw (complementary stations located upstream and downstream from the Trap stations, respectively).

Dissolved nutrients (Si, N, and P)

In the Valo Grande region (Sector V), DSi (226.62-257.46 µmol L^{-1}) was the most abundant nutrient, followed by DIN (20.55-21.81 µmol L^{-1}), DON (2.95-8.24 µmol L^{-1}), DIP (0.74-0.90 µmol L^{-1}), and DOP (0.02-0.18 µmol L^{-1}) (Figure 9a). Compared to Sector V, the southern estuarine sectors (R, C, and A) showed considerably lower nutrient concentrations. In the Batatais mangrove creek (Sector R), DSi (18.63-22.45 µmol L^{-1}) was the most abundant nutrient, followed by DON (12.91-13.72 µmol L^{-1}), DIN (1.12-1.77 µmol L^{-1}), DIP (0.40-0.51 µmol L^{-1}), and DOP (0.27-0.32 µmol L^{-1}) (Figure 9b).

In winter 2018, the Cananéia Bay (Sector C) and Ararapira Channel (Sector A) showed the same order of concentration of these nutrients (DON > DSi > DIN > DIP > DOP), with the following concentration ranges: 11.15-21.03, 8.76-23.73, 1.67-4.11, 0.53-0.75, and 0.21-0.40 µmol L^{-1} (Figure 9c) and 18.17-20.90, 6.32-8.90, 0.67-1.87, 0.26-0.51, and 0.26-0.35 µmol L^{-1}, respectively (Figure 9d). In summer 2019 (compared to winter 2018), Sector C showed a decrease in DSi and an increase in DIN, maintaining the same order of nutrient concentration (DON > DSi > DIN > DIP > DOP), with the following concentration ranges: 10.23-13.17, 3.68-7.17, 1.29-3.77, 0.18-0.66, and 0.07-0.42 µmol L^{-1} (Figure 9e). In summer 2019, Sector A experienced a considerable increase in DSi and DOP, changing the order of nutrient importance (DSi > DON > DIN > DOP > DIP), with the following concentration ranges: 14.43-47.12, 9.67-18.05, 0.81-6.64, 0.33-0.48, and 0.09-0.30 µmol L^{-1} (Figure 9f).

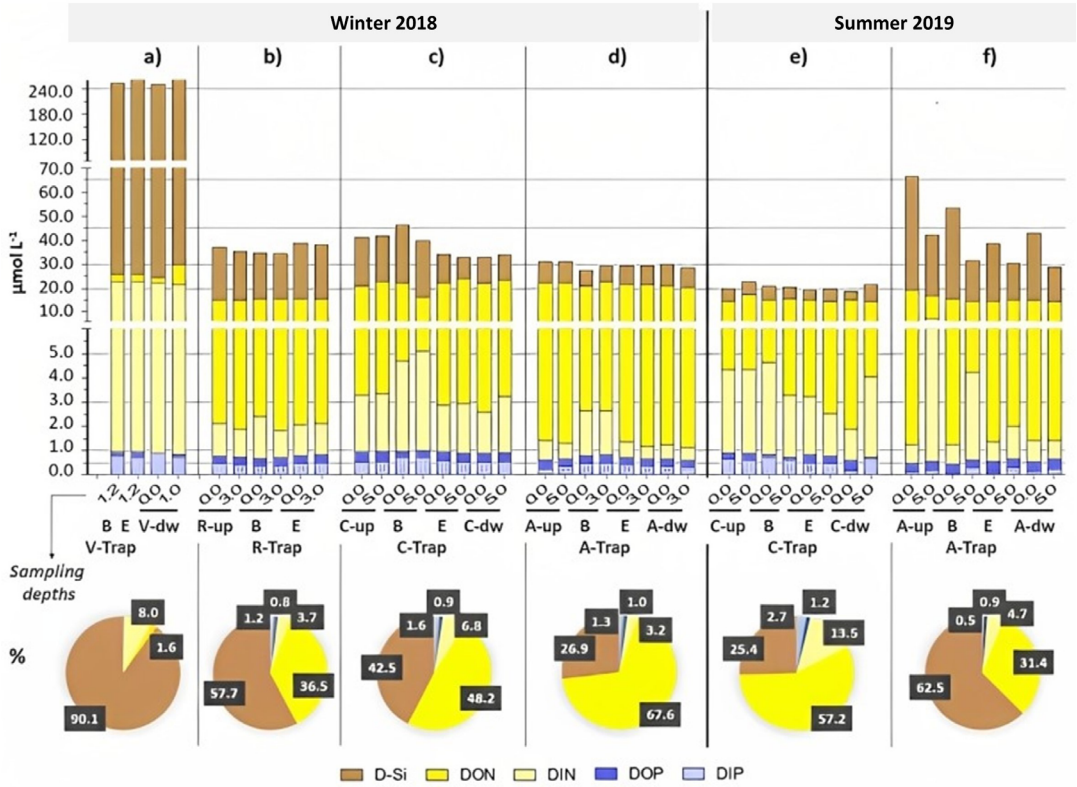

Figure 9. Stacked bar charts showing the concentration of dissolved nutrients and disc graphs expressing their ratios (% average) in the water column of the estuarine sectors: a) Valo Grande Channel (stations V); b) Batatais mangrove creek (stations R); c) and e) Cananéia Bay (stations C); and d) and f) Ararapira channel (stations A). Note: B and E (samples collected at the beginning and end of the sediment trap operation, respectively); up and dw (complementary stations located upstream and downstream from the Trap stations, respectively).

Compared to the Valo Grande region (Sector V), the southern estuarine sectors (C, R, and A) showed an increase in DON and DOP relative to DIN and DIP, respectively. DON% in TDN (Total Dissolved Nitrogen) ranged from 11.9 (V-Trap) to 28.6% (V-downstream; in winter 2018) in Sector V and from 59.3 (A-up; in summer 2019) to 97.3% (A-Trap; in winter 2018) in the southern estuarine sectors. DOP% in TDP (Total Dissolved Phosphorus) ranged from 1.8 to 19.1% in Sector V and from 15.1 (C-Trap; in summer 2019) to 83.8% (A-Trap; in summer 2019) in the southern estuarine sectors. The increase in the dissolved organic forms from the Valo Grande region (freshwater domain) to the southern sectors (surrounded by mangrove areas) was more remarkable for nitrogen than phosphorus.

Photochemical microbial activity on Dissolved Organic Matter (DOM) may release DON from humic acid (Dell'Anno et al., 1999). Millo et al. (2021), analyzing stable isotopes from sampled CIELC surface sediments, showed strong evidence that fulvic acids (the fraction of the humic substance that is soluble in acidic and basic solutions) originated from the decay of organic matter derived from local mangroves (Ararapira Channel and Cananéia Bay). Besides, it is important to note that the average concentration of DON (≈16 µmol L^{-1}) in the southern sectors resembles the annual average concentration of DON (≈20 µmol L^{-1}) found by Dittmar and Lara (2001) in a large mangrove tidal creek in Northern Brazil. The authors also reported a predominance of DON (64.5%) relative to DIN (35.5%).

Dissolved nitrogen forms (nitrate, nitrite, ammonium, and urea)

Figure 10 shows the concentrations of DIN forms (NO_3^- +, NO_2, and NH_4^+) and urea

(NH_2CONH_2). In contrast to the DIN pool, the dissolved organic nitrogen (DON) pool can be represented by a high number of chemical species in aquatic systems. In coastal waters, the increase in DIN forms can modify trophic statuses, whereas urea is an organic nitrogen form that is normally found at concentrations below 1.0 µmol L^{-1} under oligotrophic conditions and at up to 5.0 µmol L^{-1} under eutrophic conditions (Braga, 1995; Braga et al., 2017; Zhang et al., 2020). In the Valo Grande Channel (Sector V), NO_3^- (17.98-19.13 µmol L^{-1}) was the most abundant dissolved nitrogen form, followed by NH_4^+ (1.53-3.25 µmol L^{-1}), NO_2^- (0.32-0.41 µmol L^{-1}), and urea (0.21-0.42 µmol L^{-1}) (Figure 10a). Compared to Sector V, the other estuarine sectors (R, C, and A) showed considerably lower concentrations of these nitrogen forms and a higher representation of NH_4^+ within the DIN pool. In the Batatais mangrove creek (Sector R), NO_3^- (0.58-0.62) was the most abundant nitrogen form, followed by NH_4^+ (0.22-0.93 µmol L^{-1}), NO_2^- (0.24-0.27 µmol L^{-1}), and urea (0.08-0.14 µmol L^{-1}) (Figure 10b).

In winter 2018, the Cananéia Bay (Sector C) and Ararapira Channel (Sector A) showed the same order of nitrogen form concentrations (NH_4^+ > NO_3^- > urea > NO_2^-). However, concentrations (mainly of NH_4^+) were higher in Sector C: 1.24-3.11, 0.30-0.82, 0.10-0.46, and 0.13-0.23 µmol L^{-1} (Figure 10c) against 0.33-0.70, 0.14-1.19, 0.10-0.38, and 0.05-0.25 µmol L^{-1} (Figure 10d). In summer 2019 (relative to winter 2018), Sector C showed a decrease in NH_4^+ and a considerable increase in NO_3^- and urea, maintaining, however, the same order of nutrient importance (NH_4^+ > NO_3^- > urea > NO_2^-), with the following concentration ranges: 0.85-1.89, 0.19-1.96, 0.66-0.96, and 0.15-0.66 µmol L^{-1} (Figure 10e). In Sector A, samples collected in summer 2019 showed a considerable increment in NO_2^- and urea in DIN and DON pools, respectively; thus shifting the order of nitrogen form concentration (NO_3^- > NH_4^+ > urea > NO_2^-) (Figure 10f).

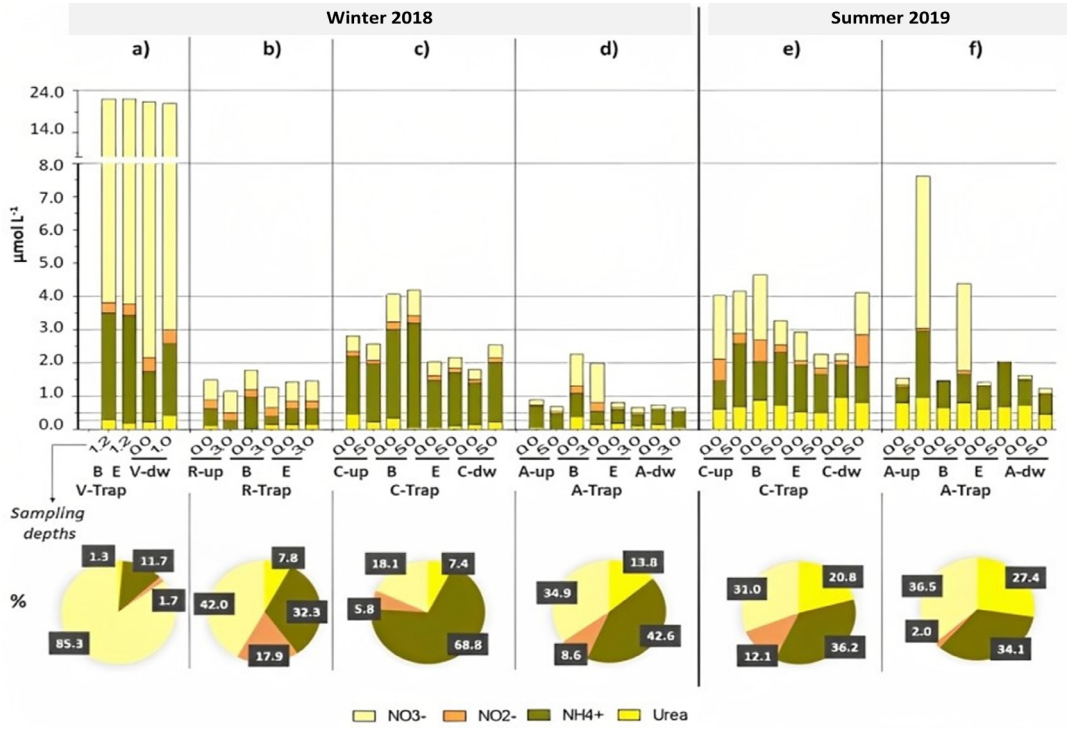

Figure 10. Stacked bar charts showing the concentration of nitrogen forms (nitrate, nitrite, ammoniacal-N, and urea) and disc graphs expressing their ratios (% average) in the water column of the estuarine sectors: a) Valo Grande Channel (stations V); b) Batatais mangrove creek (stations R); c) and e) Cananéia Bay (stations C); and d) and f) Ararapira channel (stations A). Note: B and E (samples collected at the beginning and end of the sediment trap operation, respectively); up and dw (complementary stations located upstream and downstream from the Trap stations, respectively).

Suspended Particle Matter (SPM) and its organic (POM) and inorganic (PIM) fractions

We found no considerable differences in SPM concentrations between the bottom and surface depths, except in winter 2018, when bottom waters showed relatively high SPM concentrations in the C- (88.68 mg L^{-1}) and A-Traps (86.31 mg L^{-1}) (Figure 11). Low differences in SPM occurred between the B and E sampling intervals. We observed the lowest concentration range of SPM in the Valo Grande Channel (7.72-10.71 mg L^{-1}), and the highest in the Cananéia Bay (37.00-88.68 mg L^{-1}) in winter 2018 (Figure 11).

The northern CIELC section showed the lowest concentrations of SPM (POM + PIM), with a POM range of 0.89-1.32 mg L^{-1} and a PIM range of 6.67-9.82 mg L^{-1} (Figure 11a), whereas the southern CIELC section showed considerably higher SPM concentrations. The Batatais mangrove creek had a concentration range of POM averaging 5.14-6.78 mg L^{-1}, whereas that of PIM totaled 27.00-33.57 mg L^{-1} (Figure 11b). During the winter of 2018, the Cananéia Bay showed a concentration range of POM of 6.30-10.00 mg L^{-1} and of PIM of 29.14-78.68 mg L^{-1} (Figure 11c), whereas, in summer 2019, the concentration range of POM was 8.33-12.50 mg L^{-1} and that of PIM, 24.67-34.79 mg L^{-1} (Figure 11e). The Ararapira Channel (winter 2018) showed a concentration range of POM of 6.67-14.00 mg L^{-1} and PIM of 16.25-74.57 mg L^{-1} (Figure 9d), whereas, in the summer of 2019, a concentration range of POM equal to 3.09-9.63 mg L^{-1} and of PIM, to 24.36-46.30 mg L^{-1} (Figure 11f).

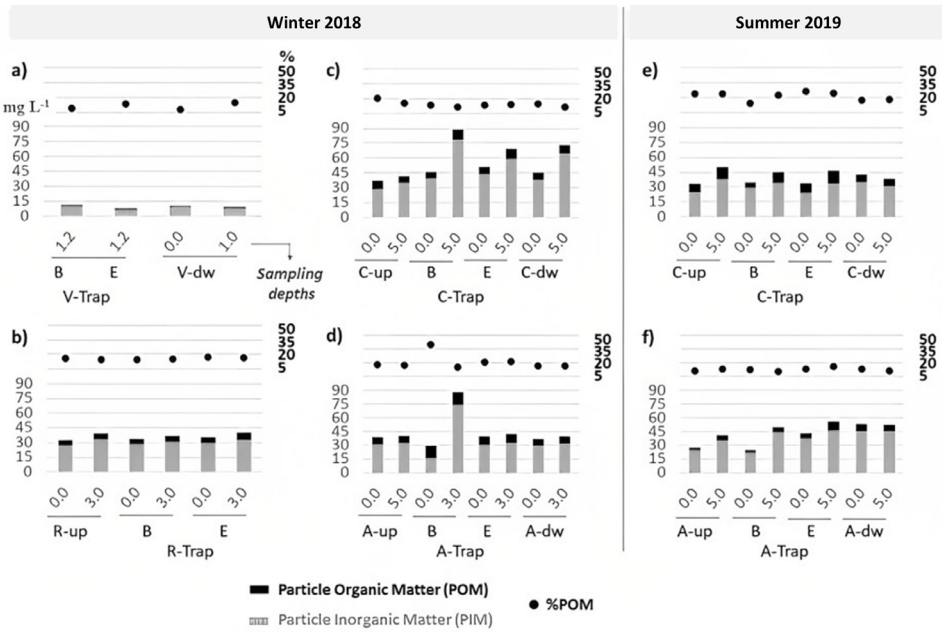

Figure 11. Concentrations of particulate organic/inorganic matter (PIM and POM) and organic matter percentages (POM%) in the water column of the estuarine sectors: a) Valo Grande Channel (stations V); b) Batatais mangrove creek (stations R); c) and e) Cananéia Bay (stations C); and d) and f) Ararapira channel (stations A). Note: B and E (samples collected at the beginning and end of the sediment trap operation, respectively); up and dw (complementary stations located upstream and downstream from the Trap stations, respectively).

POM includes living organisms (such as phytoplankton, bacteria, protozoa, and metazoan) and particulate detritus represented by organic molecules mainly based on carbon, nitrogen, and phosphorus (Emerson and Hedges, 2008). As carbon is the main element in organic compounds, POM can be estimated by the presence of POC. In turn, TEPs (Transparent Exopolymer Particles) are particles formed by the coagulation of polysaccharide fibrils, which are produced by phytoplankton, bacteria, and other microorganisms in several aquatic systems (saltwater, freshwater, and wastewater) (Alldredge et al., 1993; Passow et al., 2001). In estuaries, POM and PIM sedimentation rates are related to the amount and proprieties of such particles (i.e.,

TEPs), which undergo changes along the salinity gradient (Mari et al., 2012)

In coastal waters, PIM is primarily constituted of mineral particles (substantially represented by the most abundant elements in the Earth's crust, such as Si, Al, Fe, and Ca) that can be associated with carbon molecules. Particle Inorganic Carbon (PIC) is the smallest carbon pool on Earth and it is present in marine environments as particulate calcium carbonate ($CaCO_3$) (Hopkins et al., 2019). Thus, PIC tends to have a low representation within the PIM pool in coastal waters. Coccolithophores and foraminifera are estimated to be the dominant sources of PIC in the euphotic zone in the open ocean, whereas diatom frustules have been evinced as an important source of PIM in coastal waters (Pilskaln et al., 1996; Kostadinov et al., 2012; Zhang et al., 2014).

Photosynthetic Pigments

In the Valo Grande Channel region (Sector V), PhaeP (1.72-14.73 mg m^{-3}) was the most abundant pigment, followed by Chlc (1.51-7.49 mg m^{-3}), Chla (3.08-4.36 mg m^{-3}), and Chlb (1.12-4.51 mg m^{-3}) (Figure 12a). Compared to Sector V, the estuarine sectors (R, C, and A) of the southern section of CIELC showed considerably lower pigment concentrations and a predominance of Chla. The Batatais mangrove creek (Sector R) showed the following order of photosynthetic pigment concentration: Chla > PhaeP > Chlc > Chlb and the following ranges: 4.07-8.23, 1.51-3.59, 0.81-1.41, and 0.40-0.51 mg m^{-3} (Fig. 12b).

In winter 2018, the Cananéia Bay (Sector C) and Ararapira Channel (Sector A) showed the same order of photosynthetic pigment concentration (Chla > PhaeP > Chlc > Chlb), with the following ranges: 3.09-7.48, 1.27-4.85, 0.71-1.19, and 0.25-0.48 mg m^{-3} (Figure 12c) and 1.70-5.51, 0.28-2.26, 0.27-0.79, and 0.14-0.42 mg m^{-3} (Figure 12d), respectively. In summer 2019 (relative to winter 2018), Sector C showed a decrease in PhaeP and Chlb and an increase in Chla and Chlc. However, it maintained the same order of pigment concentration (Chla > PhaeP > Chlc > Chlb), with the following ranges: 2.46-8.51, 0.86-2.60, 0.44-1.47, and 0.12-0.32 mg m^{-3} (Figure 12e). In turn, Sector A showed an increase in all pigments in summer 2019 (relative to winter 2018), with the following concentration ranges: 4.13-9.31, 1.40-2.49, 0.47-1.44, and 0.53-1.57 mg m^{-3} (Figure 12f).

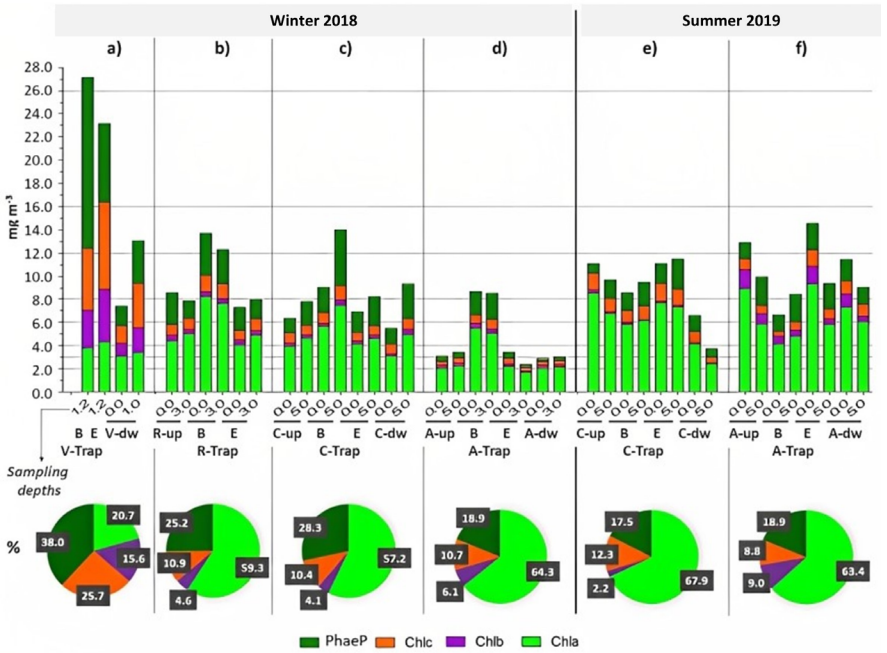

Figure 12. Stacked bar charts showing the concentration of photosynthetic pigments and disc graphs expressing their ratios (% average) in the water column of the estuarine sectors: a) Valo Grande Channel (stations V); b) Batatais mangrove creek (stations R); c) and e) Cananéia Bay (stations C); and d) and f) Ararapira channel (stations A). Note: B and E (samples collected at the beginning and end of the sediment trap operation, respectively); up and dw (complementary stations located upstream and downstream from the Trap stations, respectively).

N:P:Si ratios and Trophic State Index (TRIX)

As in oceans, we expected N:P ratios of POM (phytoplankton) in coastal waters to deviate from the Redfield ratio (16:1) (Redfield, 1958). Martiny et al. (2013) observed that the N:P ratio of POM in cold waters (high-latitude) under a nutrient-rich environment averages ~13:1, whereas, in warm waters (mid-latitude) under a nutrient-depleted environment, it amounts to ~28:1, values that are respectively lower and higher than the Redfield ratio. This may happen, for example, because diatoms require relatively nutrient-rich conditions and typically show lower-than-Redfield N:P, whereas cyanobacteria, which usually predominate in nutrient-poor regions, show higher N:P ratios (Bertilsson et al., 2003; Ho et al., 2003). Using a model of phytoplankton physiology, observational datasets, and a review of laboratory culture results, Sharoni and Halevy (2020) concluded that the Redfield ratio should be treated as the abundance-weighted sum of group-specific stoichiometry under nutrient-replete conditions, rather than as a single stoichiometric attractor. In lab experiments, Brzezinski (1985) observed that a 16:1:15 N:P:Si ratio offers the ideal growth conditions for 27 species of diatom, of which 18 (> 20 µm) showed a slightly higher mean N:Si ratio (1.2). Yet the review of Redfield et al. (1963) established a 16:1:20 N:P:Si ratio. The latter has been adopted for eutrophic coastal waters for a better understanding of eutrophication processes (Billen and Garnier, 2007; Garnier et al., 2010; Raimonet et al., 2018).

Figure 13 shows the N:P:Si (DIN:PID:DSi) ratios in the water column relative to the elemental stoichiometry of Brzezinski (1985) and Redfield et al. (1963). In this study, N:P:Si ratios remained below the limited condition ratio of 16:1:15 and 20:1:16, thereby confirming that no basic element of the habitat indicated nutrient limitation. We observed the exception at the bottom layer in the A-upstream station (Figure 13f), which showed a 23:1 N:P:Si ratio. The low N:P:Si ratios found at CIELCI resembled those in Choudhury and Bhadury (2015). These authors studied the relations between N:P:Si ratios and phytoplankton community composition in a tropical estuarine mangrove ecosystem, finding that nutrient concentrations were intricately balanced (never became limited) and complemented well Brzezinski's ratio (16:1:15). However, N:P:Si ratio deviations along estuaries can be driven by changes in trophic status (Brandini et al., 2016; Paula Filho et al., 2020) and/or in phytoplankton communities (Chai et al., 2016; Damar et al., 2020) as a result of seasonal variations in river discharges, mainly due to the high spatiotemporal variability in DSi and its control on diatom species (Conley and Malone, 1992; Conley et al., 1993; Yadav and Pandey, 2018).

Due to the high representation of silicon in terrestrial rocks and minerals, DSi is normally found at concentrations higher than DIP and DIN in estuarine systems (Braga et al., 2000; Sutti et al., 2015; Damar et al., 2020), enabling sites under nutrient-replete conditions to establish opportunist species of highly siliceous diatoms (Conley et al., 1989; Yadav and Pandey, 2018). In contrast, when DIN and DIP are discharged in excess over DSi — in relation to diatom requirements (i.e., above the N:P:Si ratio of 16:1:20) —, these will be limited, and non-diatoms will develop instead (Turner et al., 1998; Cugier et al., 2005; Billen and Garnier, 2007; Humborg et al., 2008; Chai et al., 2016; Groß et al., 2022). Investigating monthly the factors that regulate phytoplankton biomass and composition in the Patos Lagoon Estuary (south Brazilian coast), Odebrecht et al. (2018) observed that high DSi concentrations and low N:Si ratios drive diatom abundance. The analyzed CIELC estuarine sectors showed that low N:P:Si ratios (Figure 13) responded to low eutrophication levels (Figure 14), thus suggesting that diatoms were not under limiting conditions. In the case of the Valo Grande region (Sector V), the relatively low TRIX values and the high availability of DSi and nitrate evinced the occurrence of large diatom species.

In Sector V, TRIX ranged from 3.53 to 3.63, suggesting oligotrophic conditions (near the mesotrophic range) (Figure 14a). In contrast, most TRIX values found in the southern estuarine sectors remained below 3.00, configuring oligotrophic and ultra-oligotrophic conditions. The TRIX levels of the Cananéia Bay (C) and Ararapira Channel sectors showed a slight increase

from winter 2018 to summer 2019; some stations underwent a change of trophic status from ultra-oligotrophic to oligotrophic. Regarding the high nutrient concentration (mainly in nitrate) in sector V, we expected TRIX values to be considerably higher than those in the other sectors. In this case, we suggest that the high hydrodynamic driven by the Ribeira River flux (via the Valo Grande Channel) prohibits low levels of oxygen saturation, thereby disfavoring advanced stages of eutrophication in the Valo Grande Channel mouth and the adjacent estuarine area. Using a temporal data series, Cotovicz-Junior et al. (2012) showed the importance of considering the impact of salinity ranges and water residence/flushing time on the TRIX formulation in coastal environments.

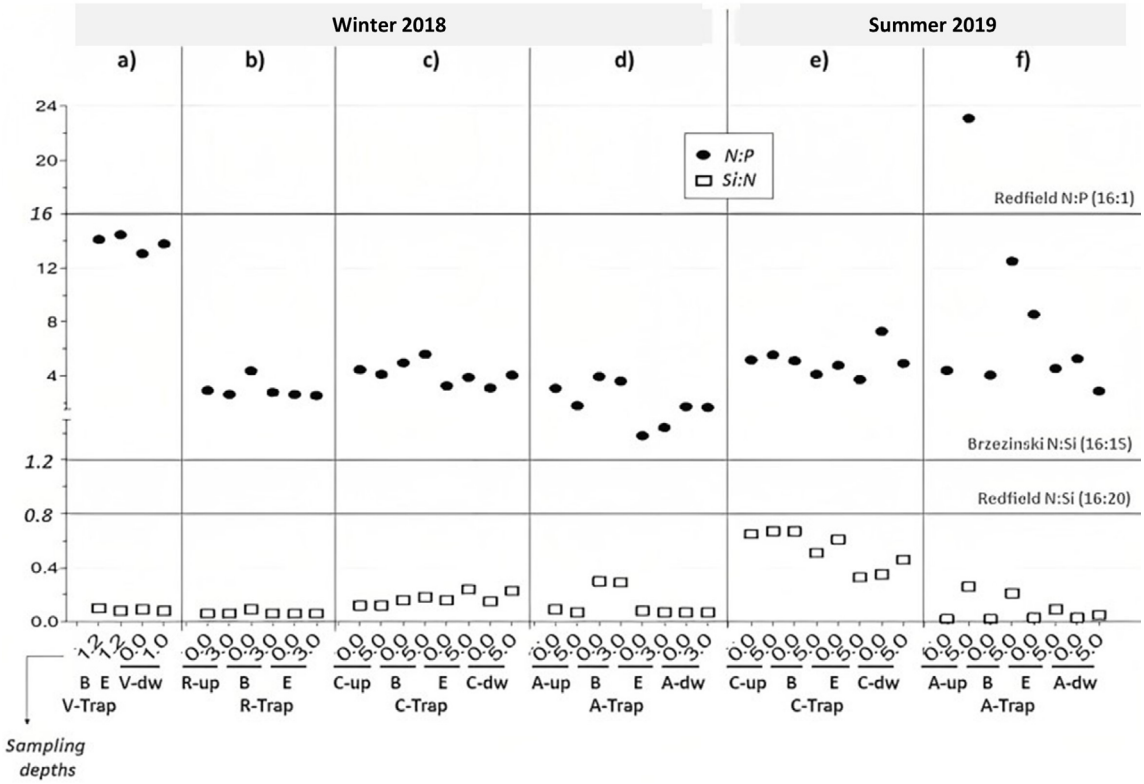

Figure 13. N:P:Si ratios in the water column of the estuarine sectors: a) Valo Grande Channel (stations V); b) Batatais mangrove creek (stations R); c) and e) Cananéia Bay (stations C); and d) and f) Ararapira channel (stations A). Note: B and E (samples collected at the beginning and end of the sediment trap operation, respectively); up and dw (complementary stations located upstream and downstream from the Trap stations, respectively). Grey lines refer to the N:P:Si ratios of marine POM established by Redfield et al. (1963) (16:1:20) and Brzezinski (1985) (16:1:15).

This study ignored the estimation of the biomass of heterotrophic bacteria, which can influence the elemental stoichiometry of marine POM (Frigstad et al., 2011). However, the bacterial effect on nitrogen transformation has been more evident in turbid and eutrophic estuaries, mostly in the sedimentary compartment (Fernandes et al., 2012; Sanders and Laanbroek, 2018). Besides, in contrast to pelagic biodiversity, benthic animals can considerably stimulate denitrification and N_2 fixation rates in estuarine sediments (Moraes et al., 2018). In eutrophic estuarine waters, denitrification and Dissimilatory Nitrate Reduction to Ammonium (DNRA) have been evinced as potential processes of nitrogen removal in turbid zones under hypoxic conditions (Zhu et al., 2018; Sutti et al., 2022). Conversely, this study showed high %DO (> 75%) and low TRIX (ultra-oligotrophic up to oligotrophic conditions) values, reflecting conditions that disfavor heterotrophic metabolism and, consequently, the denitrification and DNRA processes.

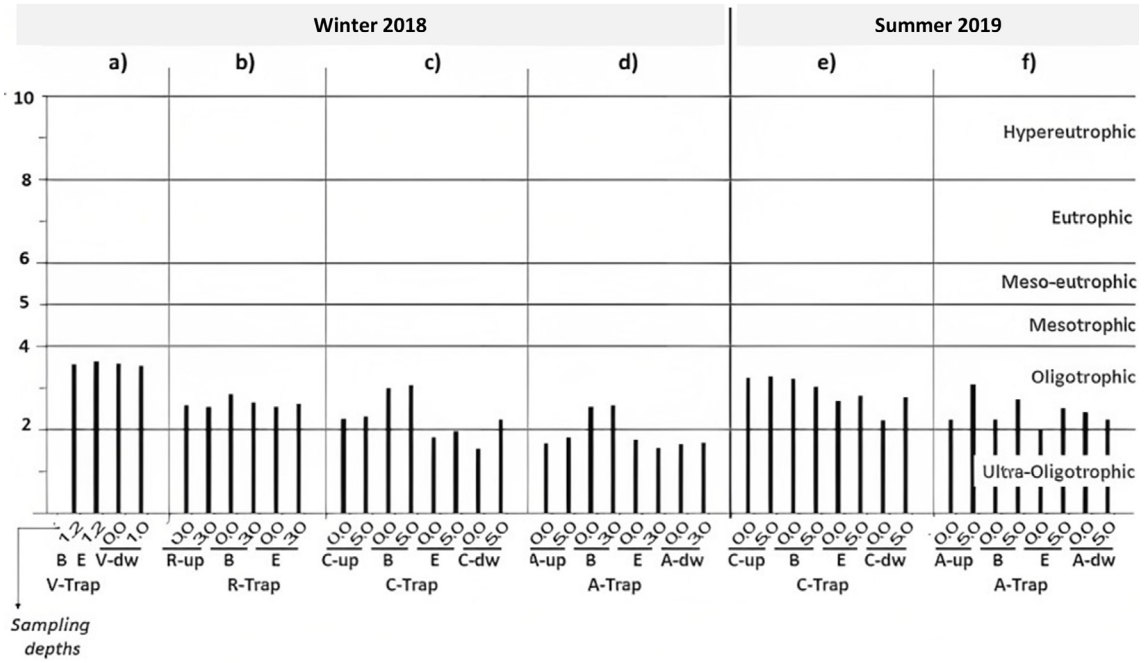

Figure 14. Trophic status (TRIX scales) of the CIELC estuarine sectors: a) Valo Grande Channel (stations V); b) Batatais mangrove creek (stations R); c) and e) Cananéia Bay (stations C); and d) and f) Ararapira channel (stations A). Note: B and E (samples collected at the beginning and end of the sediment trap operation, respectively); up and dw (complementary stations located upstream and downstream from the Trap stations, respectively).

In turn, higher DO% levels favors nitrification (aerobic oxidation of ammonium) but both nitrification and denitrification display high inhibition potential under algal blooms (Bartoli et al., 2021; Yao et al., 2021). Analyzing the intensity of bacterial activities along turbid zones, Schulz et al. (2022) observed significant nitrogen transformation by denitrifying bacteria in a tidal river with an SPM concentration higher than 1,500 mg L^{-1}, finding that nitrification significantly produces nitrate in a middle estuary with an SPM concentration higher than 200 mg L^{-1}. The estuarine sectors in this study showed considerably lower SPM concentrations, which ranged from 7.72 (Valo Grande channel) to 88.68 mg L^{-1} (Cananéia Bay). These findings suggest that the POM pool found in the photic zone of the estuarine sectors was more represented by phytoplankton than bacteria and, consequently, that bacterial activities played a low influence on N:P:Si ratios. Under an annual analysis of POM contributors (phytoplankton and bacteria) in CIELC, Mesquita and Peres (1985) found non-significant correlation factors between POM and the numerical abundance of heterotrophic particles.

Multivariate statistics and integration of particulate and dissolved forms

On the one hand, salinity is negatively correlated with dissolved inorganic nutrients (DSi, NO_3^-, and NH_4^+), accessory pigments (Chlb and Chlc), and PhaeP, thus reflecting a high inorganic nutrient input by continental drainage and showing that such nutrients drove pigment composition (Figure 15). Valo Grande discharges can lead to differences in plankton structure (Barrera-Alba et al., 2007) and microbial metabolism (decreasing the phytoplankton:bacteria ratio) (Barrera-Alba et al., 2008). On the other hand, salinity is positively correlated with particle matter (PIM and POM) and dissolved organic nutrients (DON and DOP), thus reflecting that such suspended material constituents were more pronounced in the southern estuarine sectors (those surrounded by mangrove areas), in which salinities exceeded 15. Flocculation processes in estuaries highly depend on the salinity gradient, within which big aggregates are formed in high values of salinity (Thill et al., 2001; Verney et al., 2009; Mari et al., 2012; Huang et al., 2022).

	Temp	Sal	DO%	pH	POM	PIM	DIP	DOP	DON	DSi	Urea	NH4+	TRIX	NO3-	Chla	Chlb	Chlc	PhaeP
Temp																		
Sal	0.068																	
DO%	**-0.618**	0.008																
pH	-0.011	**0.751**	0.159															
POM	0.033	**0.893**	0.124	**0.702**														
PIM	0.029	**0.813**	0.138	**0.649**	**0.789**													
DIP	**-0.383**	**-0.324**	**0.481**	0.000	-0.082	-0.171												
DOP	-0.004	**0.681**	0.038	**0.445**	**0.569**	**0.524**	**-0.528**											
DON	-0.243	**0.845**	0.277	**0.571**	**0.781**	**0.681**	-0.285	**0.670**										
DSi	-0.155	**-0.766**	-0.137	**-0.601**	**-0.869**	**-0.607**	0.009	**-0.348**	**-0.638**									
Urea	**0.885**	-0.028	**-0.542**	-0.101	-0.042	-0.083	**-0.348**	-0.041	-0.255	-0.088								
NH4+	0.135	**-0.452**	0.177	-0.290	-0.300	-0.200	**0.398**	-0.290	**-0.461**	**0.307**	0.198							
TRIX	**0.337**	**-0.532**	**-0.402**	**-0.319**	**-0.422**	**-0.416**	**0.398**	**-0.505**	**-0.741**	**0.402**	**0.316**	**0.526**						
NO3-	-0.016	**-0.567**	0.074	-0.294	**-0.414**	**-0.433**	**0.712**	**-0.580**	**-0.646**	**0.308**	0.048	**0.458**	**0.740**					
Chla	**0.493**	0.131	**-0.321**	0.119	0.120	0.180	-0.118	0.248	-0.120	0.015	**0.389**	0.213	0.001	0.139				
Chlb	0.021	**-0.685**	-0.164	**-0.641**	**-0.742**	**-0.522**	-0.137	-0.111	**-0.600**	**0.854**	0.125	0.261	0.002	0.277	0.268			
Chlc	0.138	**-0.716**	-0.084	**-0.440**	**-0.606**	**-0.560**	**0.337**	-0.286	**-0.742**	**0.594**	0.167	**0.553**	**0.727**	**0.604**	**0.467**	**0.707**		
PhaeP	0.067	**-0.435**	-0.084	-0.136	**-0.398**	-0.212	0.229	-0.078	**-0.547**	**0.529**	0.144	**0.570**	0.001	**0.494**	**0.569**	**0.628**	**0.805**	

Figure 15. Pearson correlation. Significant values at $p < 0.05$ (shaded box).

PCA established 18 factors, and the two most important factors contributed to 65% of the total observed variance. The primary factor (PC1) contributes to 43.9% of the total variance and has significant loadings on salinity and biogeochemical variables (Figure 16). In this case, continental drainage (higher in summer 2019) considerably drove the pigment composition and TRIX values of the studied estuarine sectors, whereas the presence of seawater (higher in winter 2018) increased organic (POM) and inorganic (PIM) particles and dissolved organic forms (DON and DOP).

In contrast to the Valo Grande region, the water exchanges with wetland ecosystems (mostly mangrove) in the southern estuarine sectors of CIELC (Cananéia Bay, Batatais mangrove creek, and Ararapira channel) seemed to drive, at a certain level, the lower TRIX values (oligotrophic conditions) and the predominance of DON (relative to DIN) and ammonium (within the DIN pool). In this (most preserved) CIELC area, the increase in DON could be related to the decomposition of mangrove vegetation into yellow substances (humic and fulvic acids), as evinced by Millo et al. (2021). Besides, oligotrophic mangrove creeks are areas of regeneration, thus tending to show a higher proportion of DON (relative to DIN) and ammonium (within the DIN pool) (Dittmar and Lara, 2001; Fortune et al., 2022). These biogeochemical signatures have been reported in the southern estuarine sectors under a higher influence of the high tide, which may reflect the tidal microbial dynamic in Becker et al. (2020). Under a differential abundance analysis of mangrove-associated microorganisms, these authors observed the enrichment of pelagic oligotrophic taxa during the high tide and the enrichment of putative sediment-associated microbes during the low tide. Based on this, further studies evaluating tidal microbial dynamics will help to further evaluate the influence of water exchanges with mangrove ecosystems on the trophic status, DON:DIN and N:P:Si ratios, and sinking particles in different sectors of CIELC.

The second factor (PC2) contributes to 19.1% of the observed variance and has significant loadings on temperature and biogeochemical variables (Figure 16). Under the influence of higher water temperatures in summer 2019, urea considerably increased, which, in turn, positively correlated with Chla (Figure 16). This suggests that this dissolved nitrogen form stimulated, at a certain level, the growth of primary producers and/or resulted from the biological activity of plankton in the Cananéia Bay and the Ararapira Channel. In parallel to this biogeochemical dynamic, allochthonous matter inputs (probably from river outflows) seem to have contributed to the decline in oxygen saturation (DO%).

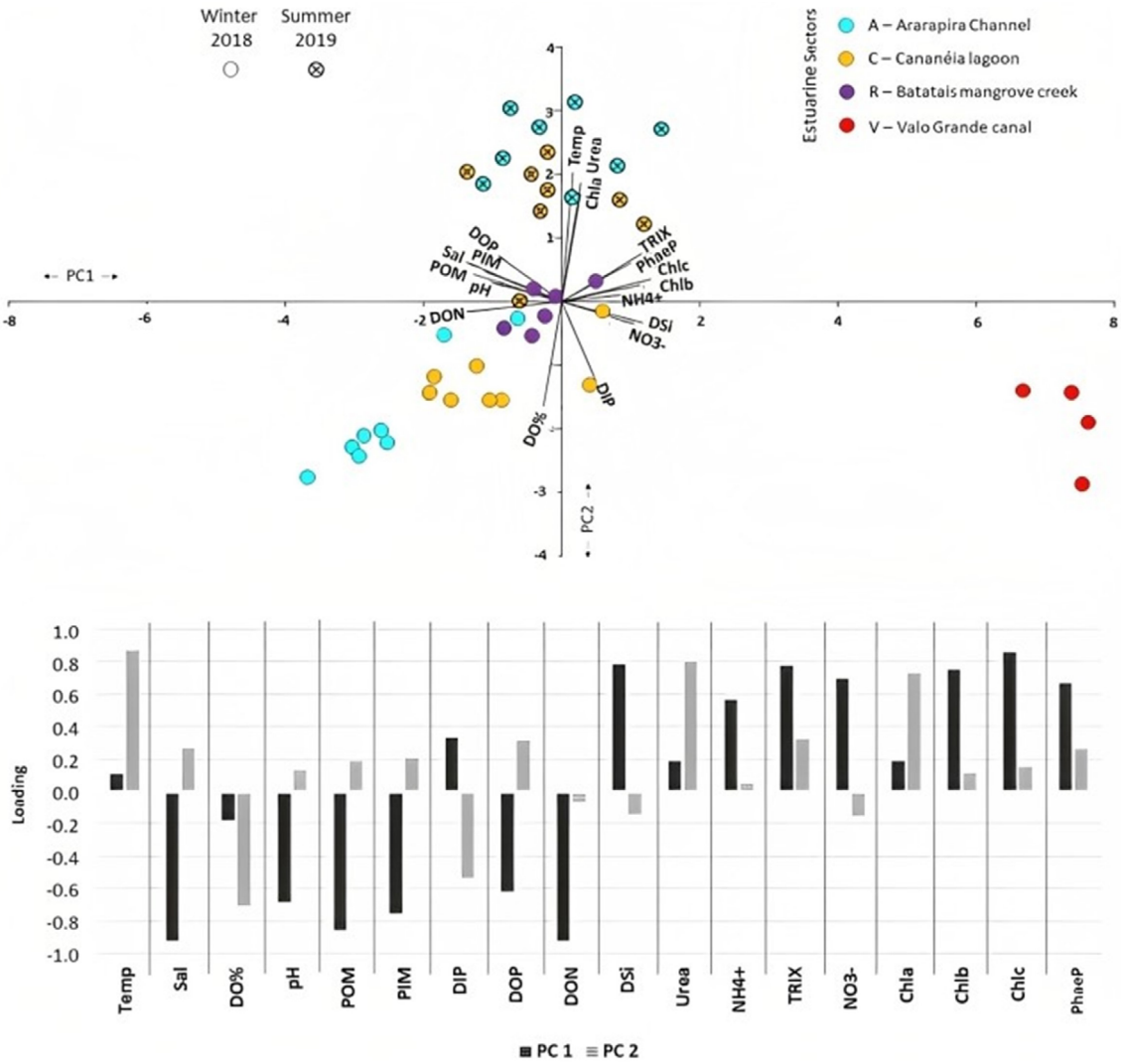

Figure 16. Principal component analysis (PCA) showing the loading pattern of the different biogeochemical parameters observed in the CIELC water columns.

Relations between photosynthetic pigments and sinking particles

Differences in the concentrations of particles (POM and PIM) and photosynthetic pigments between aquatic systems and trap collectors can inform aspects linked to sediment trap accuracy and the plankton ecology associated with sinking particles (Barlow et al., 1995; Yacobi and Ostrovsky, 2008). As Table 3 shows, the trap collectors reached considerably higher particle concentrations than those found in the water column, showing that the time scale adopted in this study was a satisfactory means of evaluating sedimentation rates. Table 3 also shows the Chla:POM ratios, which can indicate the levels of contribution of algae associated with carbon sinking (FPOM). Chla serves as an indicator of the algal content of samples because it rapidly degrades outside living cells and comprises a negligible fraction of detrital organic carbon (mainly in oxic waters) (Furlong and Carpenter, 1988). For this reason, the Chla:POM ratio is an efficient means of indicating algae association (mainly regarding the fine fraction of POM) (Hamilton et al., 2005). In contrast, when POM reaches concentrations considerably higher than Chla inside trap collectors, the phytoplankton is pointed out as a small component of the total ballasted carbon biomass in the euphotic zone (Barlow et al., 1995).

Table 3. Salinities and particle concentrations in surface waters at the beginning (B) and end (E) of the sediment trap exposure to the photic zone, as well as particle concentrations inside the trap collectors (Trap).

Station / Exp. Time	Samples	Salinity range	PIM	POM	Chla:POM	Chla	Chlb	Chlc	PhaeP
			mg L-1			mg m-3			
Winter 2018									
(V) 1.50 h	B	0.04	9.82	0.89	4.28	3.81	3.24	5.34	14.73
	Trap	---	220.76	30.91	0.84	26.08	20.27	33.15	34.16
	E	0.04	6.67	1.05	4.15	4.36	4.51	7.49	6.80
(R) 1.50 h	B	29.96	28.43	5.14	1.60	8.24	0.45	1.41	3.59
	Trap	---	434.55	283.64	0.15	41.33	4.61	6.88	26.12
	E	29.37	29.57	6.29	0.65	4.07	0.40	0.81	2.01
(C) 5.25 h	B	23.11	39.44	6.30	0.89	5.63	0.25	0.99	2.15
	Trap	---	1706.97	37.88	3.23	122.41	9.83	13.44	115.15
	E	28.64	44.18	6.73	0.61	4.12	0.31	0.71	1.78
(A) 5.75 h	B	29.85	16.25	13.00	0.42	5.51	0.42	0.75	2.01
	Trap	---	162.39	11.59	1.12	12.96	1.61	3.17	6.48
	E	29.87	31.00	9.00	0.24	2.18	0.28	0.45	0.53
Summer 2019									
(C) 4.00 h	B	18.22	29.33	4.83	1.20	5.79	0.27	0.96	1.54
	Trap	---	339.09	110.30	0.53	58.23	6.12	9.41	27.29
	E	26.65	24.17	9.33	0.82	7.65	0.24	1.47	1.75
(A) 6.50 h	B	17.10	21.81	3.19	1.29	4.13	0.65	0.47	1.41
	Trap	---	141.02	21.59	0.88	19.03	1.43	3.92	8.30
	E	23.99	37.41	5.93	1.57	9.31	1.50	1.44	2.29

Note: Valo Grande Channel (V-Trap station), Batatais mangrove creek (R-Trap station), Cananéia Bay (C-Trap station), and Ararapira channel (A-Trap station).

In this study, most Chla:POM ratios in the particulate matter inside the trap collectors remained below 1.2, except in the trap collectors in the C-Trap station (winter 2018), which showed an average ratio of 3.23 (Table 3). In subtropical estuaries, the contribution of allochthonous organic matter to the FPOM may be expressive during periods of intense river discharges, thus providing a lower algae association with SPM (i.e., under low Chla:POM ratios). In the C-Trap and A-Trap stations, the ratios inside the trap collectors were lower in summer 2019 (relative to winter 2018), which probably responded to allochthone loads driven by higher rainfall volumes. Conversely, in a semi-arid lake (Israel), in which the input of allochthonous material via freshwater inputs tends to be lower than in subtropical estuaries, Yacobi and Ostrovsky (2008) found a high contribution of algae associated with FPOM under an average Chla:POM ratio of 3.07.

Figure 17 shows the POM:PIM and Chla:b:c:PhaeP ratios in both the water column (photic zone) and trap collectors. Differences between these compartments can show the degradation/production rates of pigments. In case of degradation, the trap collectors (relative to the water column at the beginning of sediment trap exposure) should show a decrease in chlorophylls associated with an increase in PhaeP. The sediment trap set in the Valo Grande Channel (V-Trap station) showed an increase in Chla% and POM%, associated with a decrease in PhaeP% (Figure 17), evincing the contribution of primary producers to organic particle sinking (FPOM). In the R-Trap station (Batatais mangrove creek), increased percentages in PhaeP and POM

from the water column to trap collectors suggest that senescent and dead phytoplankton cells greatly contributed to the vertical flux of organic particles (FPOM).

In winter 2018, the C-Trap station (Cananéia Bay) showed a marked increase in PhaeP (relative to chlorophylls) and PIM (relative to POM) from the water column to trap collectors, whereas, in summer 2019, we observed an increase in POM% and Chlb% associated with a decrease in Chla and Chlc% (Figure 17). In winter 2018, the A-Trap station (Ararapira channel) showed a relatively high POM% value in surface waters at the beginning of the sediment trap exposure, whereas we found a marked decrease in POM% value inside the trap collectors (relative to surface waters). As observed in the C-Trap station in the summer of 2019, the A-Trap station showed an increase in POM% associated with a decrease in Chla from the water column to trap collectors (Figure 17), reflecting lower Chla:POM ratios (Table 3).

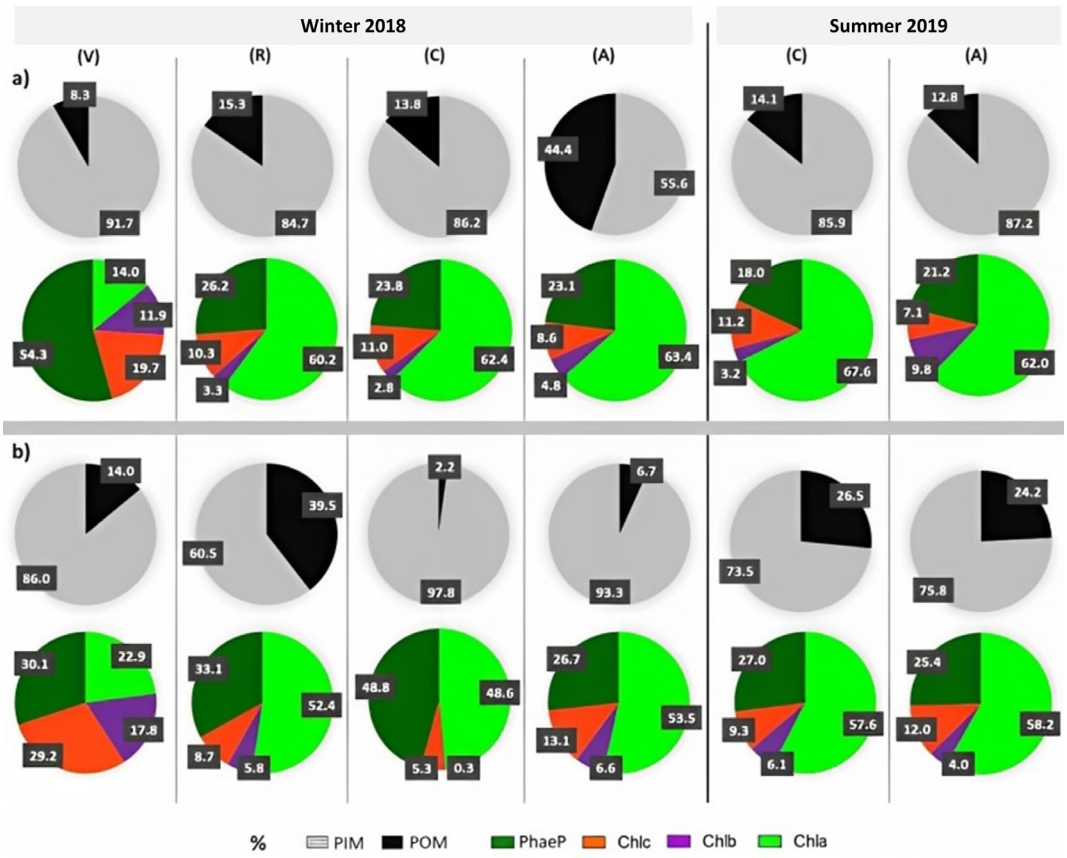

Figure 17. Proportions (%) between inorganic and organic particles (PIM and POM) and pigments (Chla, Chlb, Chlc, and PhaeP) found at: a) the surface water layer sampled at the beginning of the sediment trap exposure and b) the sediment trap collectors. Note: V-Trap station (Valo Grande Channel), R-Trap station (Batatais mangrove creek), C-Trap station (Cananéia Bay), and A-Trap station (Ararapira Channel).

The variations in the proportion of photopigments obtained by the sediment traps installed in the estuary may be accounted for by several independent processes, such as the dynamics of phytoplankton development (including predominant species and capacity of aggregation), the stability of post-produced cells in the euphotic zone (relative to their size and

physical and ecological factors), and the differential rates of preservation/decomposition of pigments. Degradation patterns depend on the interval at which degradation occurs (Louda et al., 2002). Chlb and Chlc have been evaluated as having low and high degradability inside sediment traps set in freshwater systems, respectively (Yacobi and Ostrovsky, 2008), whereas it has been shown that Chlc may be less degradable than Chla in marine cultures (Louda et al., 2002). Compared to Yacobi and Ostrovsky (2008), this study defined shorter exposure intervals for our sediment trap in the water column, thus finding lower pigment degradation/production rates inside the trap collectors.

In oceans, the zooplankton ecosystem (such as grazing and production of fecal pellets) is the most important driver of the transport of POM from the euphotic zone to deep waters (Turner, 2015). In sediment traps installed in shallow waters after days of exposure, the zooplankton ecosystem usually shows the highest contribution to the collected POM (Kähler and Bauerfeind, 2001; Buesseler et al., 2007; Honjo et al., 2008), within which Phaeopigments (PhaeP) tend to be more abundant than other pigments (Barlow et al., 1995). In contrast to aquatic systems, studies have observed high PhaeP:Clha ratios in the gut content of copepod species as a result of the destruction of chlorophylls by enzymatic activity (Head and Harris, 1996; Pandolfini, 2000; D'Souza and Gauns, 2018). This study ignored the diversity and abundance of zooplankton, thereby preventing us to recognize the species that most contributed to sinking particles. However, increased percentages in PhaeP (relative to Chla) and POM from the water column to the sediment trap content evinced large zooplankton grazing, contributing to the POM constitution in the trap collectors.

PhaeP in estuarine waters can originate from the degradation of both phytoplankton cells and land plant fragments (Mostofa et al., 2013). Estuarine waters with a high expression of vegetable detritus (by land plants) within the POM pool could be indicated by low Chla:POM and high PhaeP:Chla ratios. In contrast, when SPM is associated with high Chla:POM and Chla:PhaeP ratios, phytoplankton is pointed out as the main vegetable component of the POM pool (Hamilton et al., 2005). These ratios (measured in the photic zone during the sediment trap exposure) are useful to check the contribution level of the zooplankton ecosystem (via grazing) to carbon sinking. Significant correlations between zooplankton abundance and Chla concentration have been observed in estuarine waters (Lopes et al., 1998; Farhadian and Pouladi, 2014). The Valo Grande water column showed PhaeP concentrations higher than Chla and no increased percentages of POM and PhaeP from the water column to V-Trap collectors (Figure 17). These conditions suggest a low influence of zooplankton ecology on the F_{POM} in the V-Trap station. On the other hand, zooplankton considerably influenced F_{POM} in the R-Trap station due to the high Chla concentrations in the water column. We also found a sharp increase in POM and PhaeP% from the water column to R-Trap collectors (Figure 17). The C- and A-Trap stations showed increased percentages in POM and PhaeP (from the water column to sediment trap content) in summer 2019.

In this study, the influence of the zooplankton ecosystem on the vertical flux of organic particles could be evinced due to three methodological aspects linked to sediment trap operation: (a) no use of chemical substances to prevent "swimmers" inside the collectors, (b) sediment trap exposure at the scale of hours (1.5-6.5 h), and (c) no determination of chemical parameters from the collected material. Regarding sediment traps developed for days, the added material from the zooplankton can significantly increase the total mass of particles in traps. Therefore, in this case, swimmers should be removed and ignored in the calculation of flux (Buesseler et al., 2007). Conversely, underestimation of the vertical flux due to the loss of collected POM to solubilization can be expressive in shallow waters due to the relatively higher presence of zooplankton (in comparison with deep waters) (Honjo et al., 2008). Nevertheless, Kahler and Bauerfeind (2001), using multivariate statistics to divide solubilized organic matter in a shallow time-series trap into fractions derived from swimmers and the passive flux, observed that POM suffers significant losses to the dissolved phase after only days of exposure to the water column.

Hydrodynamic and biogeochemical drivers of particle sedimentation rates

The Valo Grande Channel (V-Trap station) sedimentation rates (vertical flux of particles) relative to PIM (F_{PIM}) and POM (F_{POM}) totaled 452.02 and 73.59 mg m^{-2} d^{-1}, respectively (Figure 18a). Regarding photosynthetic pigments, the fluxes relative to phaeopigments (F_{PhaeP}), chlorophyll-c (F_{Chlc}), chlorophyll-a (F_{Chla}), and chlorophyll-b (F_{Chlb}) reached 81.33, 78.93, 62.11, and 48.26 mg m^{-2} d^{-1}, respectively (Figure 18b). Note that the F_{PhaeP}, F_{Chlc}, and F_{Chlb} in the V-Trap station were the highest in this study. In turn, the Batatais mangrove creek (R-Trap station) showed the highest fluxes of POM (F_{POM} 675.32 mg m^{-2} d^{-1}) and Chla (F_{Chla} 98.40 mg m^{-2} d^{-1}), whereas its F_{PIM}, F_{PhaeP}, F_{Chlc}, and F_{Chlb} totaled 1034.63, 62.20, 16.38, and 10.98 mg m^{-2} d^{-1}, respectively.

In winter 2018, the Cananéia Bay (C-Trap station) showed considerable sedimentation rates in F_{PIM} (1161.20 mg m^{-2} d^{-1}), F_{Chla} (83.27 mg m^{-2} d^{-1}), and F_{PhaeP} (78.33 mg m^{-2} d-1), whereas F_{POM} (25.77 mg m^{-2} d^{-1}), F_{Chlc} (9.14 mg m^{-2} d^{-1}), and F_{Chlb} (0.45 mg m^{-2} d^{-1}) totaled relatively low rates (Figure 18). Moreover, in summer 2019, the C-Trap station showed considerably lower sedimentation rates for F_{PIM} (294.73 mg m^{-2} d^{-1}), F_{Chla} (51.99 mg m^{-2} d^{-1}), and F_{PhaeP} (24.37 mg m^{-2} d^{-1}) and considerably higher F_{POM} (106.51 mg m^{-2} d^{-1}) and F_{Chlb} (5.46 mg m^{-2} d^{-1}) rates. The Ararapira Channel (A-Trap) showed the lowest sedimentation rates (Figure 18), both in winter 2018 (F_{PIM} 100.86, F_{POM} 7.20, F_{Chla} 8.05, F_{Chlb} 1.01, F_{Chlc} 1.97, and F_{PhaeP} 4.02 mg m^{-2} d^{-1}) and summer 2019 (F_{PIM} 67.76, F_{POM} 21.59, F_{Chla} 10.46, F_{Chlb} 0.79, F_{Chlc} 2.15, and F_{PhaeP} 4.56 mg m^{-2} d^{-1}). However, compared to winter 2018, the A-Trap station showed an increase in F_{POM} and a decrease in F_{PIM} in summer 2019.

The salinity values reported at the beginning and end of sediment trap exposure are essential measures to better understand the influence of estuarine circulation (freshwater input and tidal range) on the sedimentation rates of particles, whereas the differences in particle concentrations between water column samples and sediment trap collectors may show the biogeochemical drivers of sinking particles. Table 3 also shows these variables.

Valo Grande (artificial channel)

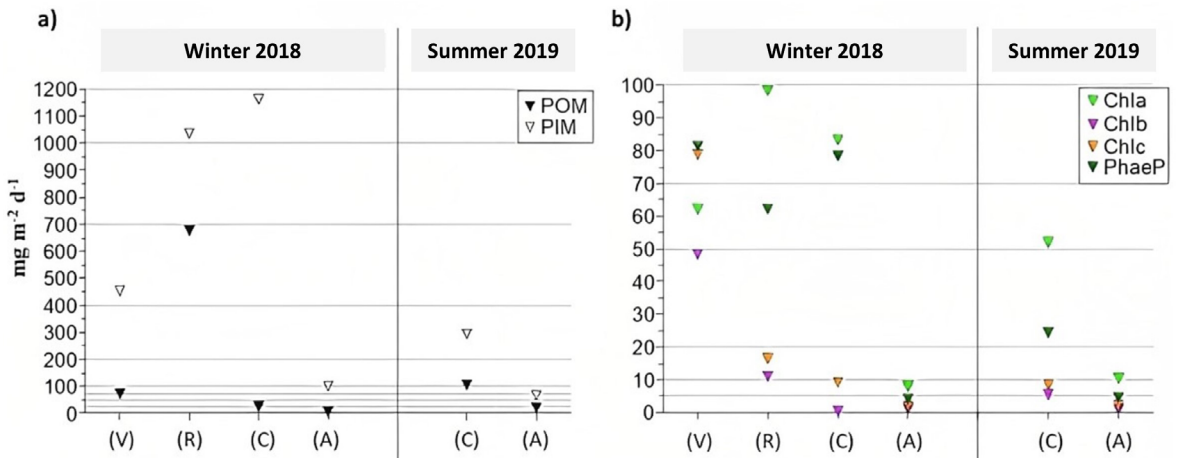

Figure 18. Particle sedimentation rates from the euphotic zone of the estuarine sectors relative to a) Organic and Inorganic Matter (PIM and POM) and b) Photosynthetic pigments (Chla, Chlb, Chlc, and PhaeP). Note: V-Trap (Valo Grande Channel); R-Trap (Batatais mangrove creek); C-Trap (Cananéia Bay); and A-Trap (Ararapira Channel).

In the Valo Grande region, the high concentrations of PhaeP and Chlb (both in the water column and sediment trap collectors) indicated a considerable presence of vegetable detritus produced by land plants and chlorophytes (green algae). This pigment composition reflected the freshwater domain (given its low salinity range — 0.01-0.04) and the high PhaeP and Chlb particle fluxes (Figure 18). Among the higher plants along the Ribeira de Iguape watershed,

floating plants (Eichhornia crassipes) have highlighted presence in the Valo Grande region. As updated by Cordeiro et al. (2020), this higher plant is listed among the 100 worst invasive plants, and CIELC features among the environmental protection areas threatened by it. The Chlb content of the photosystem II light-harvesting complex in higher plants is preserved the most (between approximately 45 and 50%) (Anderson, 1986), suggesting that Chlb contents can persist in their integrated form in higher plant detritus in freshwater environments. In addition to land plants, chlorophytes possess considerable Chlb within a double membrane-bound chloroplast, thus expressing a higher Chlb content in comparison to other phytoplankton groups both in continental and coastal environments (John, 2003; Schagerl et al., 2003; Chai et al., 2016; Damar et al., 2020). Oceans have a diversified presence of green algae, but their species are dominant in smaller size fractions (pico-plankton) and have been neglected in conceptualizing carbon cycles (Santos et al., 2016).

In comparison with land plant detritus (which probably plays a higher ballast potential), freshwater and coastal green algae represent a lower contribution to F_{POM}, F_{PhaeP}, and F_{Chlb}. This reflected the considerably lower Chla:POM ratios found in the V-trap collectors (relative to the Chla:POM ratio in the water column) (Table 3). Besides, coastal green algae (i.e., nano-phytoplankton) (Chai et al., 2016; Damar et al., 2020) on their own display a lower potential of carbon sink (F_{POM}) than diatoms (i.e., micro-phytoplankton). This study has no analytical structure (e.g., microscopic phytoplankton analysis and determination of biogenic silica) to quantify diatom contribution to sinking particles. Nevertheless, the increased percentages in Chla and POM inside the V-Trap collectors (relative to the water column), in association with the marked concentrations in SiD and nitrate found in the water column, suggest that large diatoms may also have represented an important contribution to F_{POM}. In the Valo Grande region, *S. cf. costatum* (an opportunist diatom) has been estimated to show high density and abundance (> 90%) (Kutner, 1972; Barrera-Alba and Moser, 2016). Furthermore, we observed no increase in PhaeP% (in association with the increase in POM%) from the water column to V-Trap collectors, suggesting that the contribution of zooplankton ecosystems to F_{POM} was considerably lower than that of vegetable detritus and phytoplankton. When the Valo Grande Channel was reopened in the 1980s, copepod species (20-150 µm) considerably declined in the adjacent estuarine area (i.e., the Mar Pequeno estuarine channel) (Almeida Prado et al., 1989).

Batatais mangrove creek

The Batatais mangrove creek (Sector R) showed high POM (675.32 mg m^{-2} d^{-1}), Chla (98.40 mg m^{-2} d^{-1}), and PhaeP (62.20 mg m^{-2} d^{-1}) sedimentation rates (Figure 18). In tropical estuaries, isotopic analysis ($\delta^{13}C$/ $\delta^{12}C$) has shown that mangrove tree detritus is an important source of POM in riverine sites and of marine algae in lower zones (Sarma et al., 2012; Saavedra-Hortua et al., 2020). In the R-Trap station, the contribution of mangrove tree detritus to particle sedimentation rates seemed to be considerably lower than the plankton contribution. The surface waters of the R-Trap station showed the highest range of Chla (4.1-8.2 mg m^{-3}), and the increased percentages in POM and PhaeP inside the R-Trap collectors (relative to the water column) suggested high contributions of phytoplankton senescent cells and zooplankton ecosystem to sinking particles. This result reflected the lower Chla:POM ratios in the R-Trap collectors (relative to the water column) (Table 3).

Copepod species are the principal component of the zooplankton community in CIELC, in which periods of backwaters in mangrove creeks provide good conditions for reproduction and growth (Ara, 2001a, 2001b; Tundisi and Matsumura-Tundisi, 2001). Near the studied region, in the Paranaguá estuarine complex (≈100 km south of CIELC), the maximum abundances (10,000-80,000 C m^{-3}) of copepod species occurred under high values of salinity (20-30) and Chla (up to 7.0 mg m^{-3}) (Lopes et al., 1998). The Batatais mangrove creek changes waters with the lower zone of the Cananéia Bay, thereby reflecting its high salinities (≈30). Moreover, the marine influence on the biogeochemical variables found in the R-Trap station may have been even higher since the sampling period occurred just after the high tide.

Cananéia Bay

In the Cananéia Bay, it is important to consider some seasonal differences, such as higher values of salinity, SPM (POM + PIM), F_{SPM} (F_{POM} + F_{PIM}), and SID observed in winter 2018 (19.3-19.7 °C water temperature range). The highest sedimentation rate in SPM (1,186.97 mg m^{-2} d^{-1}) was probably favored by aggregation processes during the salinity increase (from 23.90 to 28.64 in surface waters) along the flooding phase of a spring tide. In addition to the polysaccharides (essential for the coagulation process) produced by plankton components, aggregation dynamics and vertical particle flux in estuaries highly depend on salinity gradient (Thill et al., 2001; Verney et al., 2009). The salinity range (23-28), associated with the highest sedimentation rate in this study (Figure 18) reflected the results of the robust investigation by Mari et al. (2012) on the role of TEPs (Transparent Exopolymer Particles) in the aggregation dynamics along the salinity gradient of a tropical estuary. These authors found that aggregation processes were highly stimulated by an increase in TEPs at a salinity range of 10-15, whereas big aggregates and maximum sedimentation rates occurred at salinities above 23.

The highest sedimentation rate in SPM was marked by an expressive inorganic representation (FPIM = 1161.20 mg m^{-2} d^{-1}), which was associated with high vertical fluxes in Chla and PhaeP (Figure 18). These results show that both mineral and biogenic particles were important to F_{PIM}. The high importance of phytoplankton to F_{SPM} is also evinced by the highest Chla:POM ratio (3.23) found in C-Trap collectors (Table 3). Moreover, C-Trap collectors showed no POM% increase (together with the increase in PhaeP%) regarding that in the water column, thereby evincing a low influence of the zooplankton ecosystem on sinking particles. Thus, we suggest that this expressive vertical flux of inorganic particles (F_{PIM}), associated with a high vertical flux of Chla (Figure 18), had a considerable contribution from biogenic silica.

In the summer of 2019 (27.2-28.2 °C water temperature range), the SPM sedimentation rate (401.24 mg m^{-2} d^{-1}) was considerably lower but with a higher organic representation (F_{POM} = 106.51 mg m^{-2} d^{-1}). This higher organic expression in sinking particles may have responded to the zooplankton ecosystem since we observed greater PhaeP and POM percentages from the water column to C-Trap collectors (Figure 17). These results, in turn, reflected the lower Chla:POM ratios observed in the C-Trap collectors (relative to the water column) (Table 3). In the lower zone of the Cananéia Bay, Ara (2001a) found that water temperatures above 20°C increased the reproduction rates (daily egg production) of copepods.

Under neap tide conditions, the C-Trap was developed during the final local flood phase and during high tides. These tidal conditions — recorded in the summer of 2019 —, in association with higher rainfall volumes, configured a period with a lower salinity range (18.22-21.65 in surface waters) and haline stratification. This hydrodynamic condition probably disfavored high sedimentation rates, reflecting the lower values in F_{SPM} (compared to the winter of 2018). Huang et al. (2022) found that a low salinity condition during a haline stratification period significantly decreased the formation of macro-flocs (big aggregates) in the Modaomen Estuary (Chinese subtropical coast).

Ararapira Channel

The central region of the Ararapira Channel showed the lowest nutrient levels (ultra-oligotrophic condition), associated with an N:P ratio near the Redfield ratio (16:1), evincing an estuarine region prone to establishing nutrient-limited conditions. Despite the considerable Chla concentrations (2.18-9.31 mg m^{-3}) recorded in the water column, it showed the lowest vertical fluxes of SPM (< 110 mg m^{-2} d^{-1}) and photosynthetic pigments (< 20 mg m^{-2} d^{-1}) in both seasons (Figure 18). Furthermore, PhaeP% and POM% values showed no considerable increases from the water column to the A-Trap collectors (Figure 17). These results indicate that the low presence of micro-plankton (favored by ultra-oligotrophic conditions) was highly related to the lowest sedimentation rates. In the case of summer 2019, N:P ratios were even closer to the Redfield ratio.

In addition to biogeochemical drivers, hydrodynamic drivers may have contributed to the lowest sedimentation rates. Despite the high salinities (29.85-31.11) found in winter 2018, they showed no considerable increase in salinity during the tidal phase (high tide and beginning of the ebb tide) to which the A-Trap was exposed. This hydrodynamic condition probably disfavored aggregation processes. In estuaries, these processes also depend on particle collision rates (Thill et al., 2001; Mari et al., 2012), which may be low in low hydrodynamic periods (e. g., under neap tides and during tidal phase transition).

CONCLUSION

The results of this study show important insights concerning the physical and biogeochemical dynamics of suspended material (considering dissolved/particulate and inorganic/organic fractions) and its impact on sedimentation rates in different sectors of the CIELC. The exposure times (1.5-6.5 h) adopted to set the cylindrical sediment trap in the photic zone provided a large number of collected particles (considerably higher than the particle concentration reported in the water column), which suffered relatively low pigment degradation and low production of organic particles inside the trap collectors. These conditions enable us to point out the contribution levels of plankton ecological interactions to particle vertical fluxes. Further studies in CIELC must verify the abundance and diversity of plankton components in sediment trap contents in parallel to the analysis of degradation/production rates (concerning the different concentrations of SPM and pigments observed between the water column and trap collectors) to better understand the influence of plankton ecological interactions on sinking particles. Besides, the determination of stable isotopes from the material collected by sediment traps may provide a better understanding of the contribution of macrophytes to particle sedimentation rates.

In the Valo Grande region, high silicate and nitrate concentrations associated with high vertical fluxes in the phaeopigments Chla and Chlb evinced vegetable species (both macro- and microalgae) as an important biogeochemical driver to sinking particles. The Batatais mangrove creek showed the highest vertical fluxes in POM and Chla, evincing an aquatic ecosystem with high carbon sequestration potential. In the lower zone of the Cananéia Bay, flocculation processes were pointed out as the main driver of the highest particle sedimentation rate reported in winter 2018 during the flood tide phase of a spring tide, which was marked by a homogenous water column (no stratification) and a considerable increase in salinity. On the other hand, the lower particle sedimentation rate observed in summer 2019 seemed to have responded to low flocculation intensities since the sediment trap operated within a period under haline stratification and lower salinities. A more detailed comprehension about particle sedimentation in CIELC requires more knowledge of the density stratification and flocculation phenomenon along salinity gradients. The central region of the Ararapira channel showed the lowest particle sedimentation rates, which were associated in both seasons with low nutrient levels, ultra-oligotrophic conditions, and N:P ratios close to 16:1 (Redfield ratio), thereby evincing a low influence of micro-phytoplankton on sinking particles.

Finally, one coastal area so complex as this studied system tends to show considerable spatial and seasonal differences in the vertical fluxes of particles in its productive layer (euphotic zone). Freshwater and saltwater inputs were pointed out as important controls of biogeochemical properties (including trophic conditions) and particle sedimentation rates that, in turn, responded to different levels of preservation and anthropogenic influence.

ACKNOWLEDGMENTS

The authors would like to thank the financial support of CNPq (310624/2016-9-7), FAPESP (2020/16485-7 and 2018/08738 -2), and CAPES (Financing Code 001), as well as the efforts of the RV Alabacora crew and team of the Research Base of Cananéia for providing good conditions for workplaces. We also thank the team of the Laboratory of Nutrients, micronutrients, and traces in the Oceans (LABNUT-IOUSP) and the essential support of the Oceanographic Institute of the University of São Paulo.

AUTHOR CONTRIBUTIONS

B.O.S.: Conceptualization; Writing – original draft; Investigation, Writing – review & editing;

V.G.C.: Methodology; Formal Analysis.

C.G.C.: Methodology; Writing – review & editing;

E.S.B.: Supervision; Resources; Project Administration; Investigation; Funding Acquisition; Writing – review & editing.

REFERENCES

Alldredge, A. L., Passow, U. & Logan, B. E. 1993. The abundance and significance of a class of large, transparent organic particles in the ocean. *Deep Sea Research Part I: Oceanographic Research Papers*, *40*(6), 1131–1140. DOI: https://doi.org/10.1016/0967-0637(93)90129-q

Almeida Prado, M. S., Pompeu, M. & Porto, F. D. 1989. Environmental quality and ecosystem stability. *In*: Spanier, Y., Steinberg, S., & Luria, M. (eds.). Jerusalem: ISEEQS Pub.

Aminot, A. & Chaussepied, M. 1983. *Manuel des analyses chimiques en milieu marin*. Paris: Editions Jouve.

Anderson, J. M. 1986. Photoregulation of the Composition, Function, and Structure of Thylakoid Membranes. *Annual Review of Plant Physiology*, *37*(1), 93–136. DOI: https://doi.org/10.1146/annurev.pp.37.060186.000521

Angulo, R. J., Souza, M. C. de, Sielski, L. H., Nogueira, R. A. & Müller, M. E. J. 2019. Morphology, bedforms andbottom sediments of Mar do Ararapira, southern Brazil. *Quaternary and Environmental Geoscience*, *10*(1), 1–9.

Ara, K. 2001a. Daily egg production rate of the planktonic calanoid copepod Acartia lilljeborgi Giesbrecht in the Cananéia Lagoon estuarine system, São Paulo, Brazil. *Hydrobiologia*, *445*(1/3), 205–215. DOI: https://doi.org/10.1023/a:1017573917281

Ara, K. 2001b. Temporal variability and production of the planktoniccopepods in the Cananeia Lagoon estuarine system,Sao Paulo, Brazil. II. Acartia lilljeborgi. *Plankton Biology & Ecology*, *48*(1), 35–45.

Arasaki, E. & Alfredini, P. 2009. *Obras e gestão de portos e costas* (2nd ed.). São Paulo: Blucher.

Armstrong, F. A. J., Williams, P. M. & Strickland, J. D. H. 1966. Photooxidation of organic matter in seawater by ultraviolet radiation analytical and application. *Nature*, 211, 463-481

Azevedo, J. de S. & Braga, E. S. 2011. Caracterização hidroquímica para qualificação ambiental dos estuários de Santos-São Vicente e Cananéia. *Arquivos de Ciências Do Mar*, *44*(2), 52–61.

Baker, E. T., Milburn, H. B. & Tennant, D. A. 1988. Field assessment of sediment trap efficiency under varying flow conditions. *Journal of Marine Research*, *46*, 573–592.

Bale, A. J. 1998. Sediment trap performance in tidal waters: comparison of cylindrical and conical collectors. *Continental Shelf Research*, *18*(11), 1401–1418. DOI: https://doi.org/10.1016/s0278-4343(98)00050-8

Barlow, R. G., Mantoura, R. F. C., Peinert, R. D., Miller, A. E. J. & Fileman, T. W. 1995. Distribution, sedimentation and fate of pigment biomarkers following thermal stratification in the western Alboran Sea. *Marine Ecology Progress Series*, *125*(1/3), 279–291.

Barrera-Alba, J. J., Gianesella, S. M. F., Moser, G. A. O. & Saldanha-Corrêa, F. M. P. 2008. Bacterial and phytoplankton dynamics in a sub-tropical estuary. *Hydrobiologia*, *598*(1), 229–246. DOI: https://doi.org/10.1007/s10750-007-9156-4

Barrera-Alba, J. J., Gianesella, S. M. F., Saldanha-Corrêa, F. M. P. & Moser, G. A. O. 2007. Influence of an Artificial Channel in a Well-Preserved Sub-Tropical Estuary. *Journal of Coastal Research*, (50), 1137–1141.

Barrera-Alba, J. J. & Moser, G. A. O. 2016. Short-term response of phytoplankton community to over-enrichment of nutrients in a well-preserved subtropical estuary. *Brazilian Journal of Oceanography*, 64(2), 191-196.

Bartoli, M., Nizzoli, D., Zilius, M., Bresciani, M., Pusceddu, A., Bianchelli, S., Sundbäck, K., Razinkovas-Baziukas, A. & Viaroli, P. 2021. Denitrification, Nitrogen Uptake, and Organic Matter Quality Undergo Different Seasonality in Sandy and Muddy Sediments of a Turbid Estuary. *Frontiers in Microbiology*, *11*. DOI: https://doi.org/10.3389/fmicb.2020.612700

Becker, C. C., Weber, L., Suca, J. J., Llopiz, J. K., Mooney, T. A. & Apprill, A. 2020. Microbial and nutrient dynamics in mangrove, reef, and seagrass waters over tidal and diurnal time scales. *Aquatic Microbial Ecology*, *85*, 101–119. DOI: https://doi.org/10.3354/ame01944

Beltran, E. V., Sutti, B. O., Gonçalves, E. L., Reis, F. C., Oliveira, W. R. L. de, Schaefer, F., Clara, M. M., Giordano, F. & Barrella, W. 2012. Estimativa do Sequestro de Carbono por Árvores de Manguezal no RioBoturoca – São Vicente/SP. *UNISANTA BioScience*, *1*(1), 11–15.

Bertilsson, S., Berglund, O., Karl, D. M. & Chisholm, S. W. 2003. Elemental composition of marine *Prochlorococcus* and *Synechococcus*: Implications for the ecological stoichiometry of the sea. *Limnology and Oceanography*, *48*(5), 1721–1731. DOI: https://doi.org/10.4319/lo.2003.48.5.1721

Bianchi, T. S. 2006. *Biogeochemistry of Estuaries*. Oxford University Press. DOI: https://doi.org/10.1093/oso/9780195160826.001.0001

Billen, G. & Garnier, J. 2006. River basin nutrient delivery to the coastal sea: Assessing its potential to sustain new production of non-siliceous algae. *Marine Chemistry*, *106*(1–2), 148–160. DOI: https://doi.org/10.1016/j.marchem.2006.12.017

Braga, E. de S. 2020. Total Dissolved Nitrogen and Phosphorus Determination inCoastal South Atlantic Water Based on UV Oxidation Method. *American Journal of Sciences and Engineering Research*, *3*(6), 60–66.

Braga, E. de S., Berbel, G. B. B., Chiozzini, V. G. & Andrade, N. C. G. 2017. Dissolved organic nutrients (C, N, P) in seawater on the continental shelf in the Southwestern South Atlantic with emphasis State Marine Park of Laje de Santos (SMPLS) - São Paulo - Brazil. *Brazilian Journal of Oceanography*, *65*(4), 614–627. DOI: https://doi.org/10.1590/s1679-87592017136506504

Braga, E. S. 1995. Distribuição sazonal da ureia na região de Ubatuba 45° 04´W e 23° 32´S. *Boletim Do Instituto Oceanográfico*, *11*, 91–98.

Braga, E. S., Bonetti, C. V. D. H., Burone, L. & Filho, J. B. 2000. Eutrophication and Bacterial Pollution Caused by

Industrial and Domestic Wastes at the Baixada Santista Estuarine System – Brazil. *Marine Pollution Bulletin*, *40*(2), 165–173. DOI: https://doi.org/10.1016/s0025-326x(99)00199-x

Brandini, N., Rodrigues, A. P. de C., Abreu, I. M., Junior, L. C. C., Knoppers, B. A. & Machado, W. 2016. Nutrient behavior in a highly-eutrophicated tropical estuarine system. *Acta Limnologica Brasiliensia*, *28*(0). DOI: https://doi.org/10.1590/s2179-975x3416

Breitburg, D. 2002. Effects of hypoxia, and the balance between hypoxia and enrichment, on coastal fishes and fisheries. *Estuaries*, *25*(4), 767–781. DOI: https://doi.org/10.1007/bf02804904

Brewin, R. J. W., Sathyendranath, S., Platt, T., Bouman, H., Ciavatta, S., Dall'Olmo, G., Dingle, J., Groom, S., Jönsson, B., Kostadinov, T. S., Kulk, G., Laine, M., Martínez-Vicente, V., Psarra, S., Raitsos, D. E., Richardson, K., Rio, M.-H., Rousseaux, C. S., Salisbury, J., Shutler, J. D. & Walker, P. 2021. Sensing the ocean biological carbon pump from space: A review of capabilities, concepts, research gaps and future developments. *Earth-Science Reviews*, *217*, 103604. DOI: https://doi.org/10.1016/j.earscirev.2021.103604

Brzezinski, M. A. 1985. The Si:C:N ratio of marine diatoms: interspecific variability and the effect of some environmental variables. *Journal of Phycology*, *21*(3), 347–357. DOI: https://doi.org/10.1111/j.0022-3646.1985.00347.x

Buesseler, K. O., Antia, A. N., Chen, M., Fowler, S. W., Gardner, W. D., Gustafsson, O., Harada, K., Michaels, A. F., Loeff, M. R. van der, Sarin, M., Steinberg, D. K. & Trull, T. 2007. An assessment of the use of sediment traps for estimatingupper ocean particle fluxes. *Journal of Marine Research*, *65*, 345–416.

Chai, C., Jiang, T., Cen, J., Ge, W. & Lu, S. 2016. Phytoplankton pigments and functional community structure in relation to environmental factors in the Pearl River Estuary. *Oceanologia*, *58*(3), 201–211. DOI: https://doi.org/10.1016/j.oceano.2016.03.001

Chislock, M. F., Doster, E., Zitomer, R. A. & Wilson, A. E. 2013. Eutrophication: Causes, Consequences, and Controls in Aquatic Ecosystems. *Nature Education Knowledge*, *4*(4), 10.

Choudhury, A. K. & Bhadury, P. 2015. Relationship between N : P : Si ratio and phytoplankton community composition in a tropical estuarine mangrove ecosystem. *Biogeosciences Discussions*, *12*, 2307–2355. DOI: https://doi.org/10.5194/bgd-12-2307-2015

Cole, J. J., Prairie, Y. T., Caraco, N. F., McDowell, W. H., Tranvik, L. J., Striegl, R. G., Duarte, C. M., Kortelainen, P., Downing, J. A., Middelburg, J. J. & Melack, J. 2007. Plumbing the Global Carbon Cycle: Integrating Inland Waters into the Terrestrial Carbon Budget. *Ecosystems*, *10*(1), 172–185. DOI: https://doi.org/10.1007/s10021-006-9013-8

Conley, D. J., Kilham, S. S. & Theriot, E. 1989. Differences in silica content between marine and freshwater diatoms. *Limnology and Oceanography*, *34*(1), 205–212. DOI: https://doi.org/10.4319/lo.1989.34.1.0205

Conley, D. J. & Malone, T. C. 1992. Annual Cycle of Dissolved Silicate in Chesapeake Bay: Implications for the Production and Fate of Phytoplankton Biomass. *Marine Ecology Progress Series*, *81*, 121–128.

Conley, D. J., Schelske, C. L. & Stoermer, E. F. 1993. Modification of the biogeochemical cycle of silica with eutrophication. *Marine Ecologogy Progress Series*, *101*, 179–192.

Cordeiro, P. F., Goulart, F. F., Macedo, D. R., Campos, M. D. C. S. & Castro, S. R. 2020. Modeling of the potential distribution of Eichhornia crassipes on a global scale: risks and threats to water ecosystems. *Ambiente e Agua - An Interdisciplinary Journal of Applied Science*, *15*(2), 1. DOI: https://doi.org/10.4136/ambi-agua.2421

Cotovicz Junior, L. C., Brandini, N., Knoppers, B. A., Mizerkowski, B. D., Sterza, J. M., Ovalle, A. R. C. & Medeiros, P. R. P. 2012. Assessment of the trophic status of four coastal lagoons and one estuarine delta, eastern Brazil. *Environmental Monitoring and Assessment*, *185*(4), 3297–3311. DOI: https://doi.org/10.1007/s10661-012-2791-x

Cugier, P., Billen, G., Guillaud, J. F., Garnier, J. & Ménesguen, A. 2005. Modelling the eutrophication of the Seine Bight (France) under historical, present and future riverine nutrient loading. *Journal of Hydrology*, *304*(1–4), 381–396. DOI: https://doi.org/10.1016/j.jhydrol.2004.07.049

Damar, A., Colijn, F., Hesse, K.-J. & Kurniawan, F. 2020. Coastal Phytoplankton Pigments Composition in Three Tropical Estuaries of Indonesia. *Journal of Marine Science and Engineering*, *8*(5), 311. DOI: https://doi.org/10.3390/jmse8050311

Dell'Anno, A., Fabiano, M., Bompadre, S., Armeni, M., Leone, L. & Danovaro, R. 1999. Phytopigment and DNA determinations in long-time formalin-preserved trap samples. *Marine Ecology Progress Series*, *191*, 71–77.

Dittmar, T. & Lara, R. J. 2001. Driving Forces Behind Nutrient and Organic Matter Dynamics in a Mangrove Tidal Creek in North Brazil. *Estuarine, Coastal and Shelf Science*, *52*(2), 249–259. DOI: https://doi.org/10.1006/ecss.2000.0743

D'Souza, A. M. & Gauns, M. U. 2018. Temporal variability in copepod gut pigments over the central western continental shelf of India. *Journal of the Marine Biological Association of the United Kingdom*, *98*(1), 149–159. DOI: https://doi.org/10.1017/s0025315416001144

Emerson, S. & Hedges, J. 2008. Life processes in the ocean. *In*: Emerson, S. & Hedges, J. (eds.), *Chemical Oceanography and the Marine Carbon Cycle* (pp. 173–218). Cambridge University Press. DOI: https://doi.org/10.1017/cbo9780511793202.007

Farhadian, O. & Pouladi, M. 2014. Seasonal changes in the abundance and biomass of zooplankton from shallow mudflat river-estuarine system in Persian Gulf. *Brazilian Journal of Aquatic Science and Technology*, *18*(2), 19–29. DOI: https://doi.org/10.14210/bjast.v18n2.p19-29

Fernandes, S. O., Michotey, V. D., Guasco, S., Bonin, P. C. & Bharathi, P. A. L. 2012. Denitrification prevails over anammox in tropical mangrove sediments (Goa, India). *Marine Environmental Research*, *74*, 9–19. DOI: https://doi.org/10.1016/j.marenvres.2011.11.008

Fortune, J., Kaestli, M., Butler, E. C. V. & Gibb, K. 2022. Denitrification in intertidal sediments of a tropical estuary subject to increasing development pressures. *Aquatic Sciences*, *84*(4). DOI: https://doi.org/10.1007/s00027-022-00885-0

Frigstad, H., Andersen, T., Hessen, D. O., Naustvoll, L.-J., Johnsen, T. M. & Bellerby, R. G. J. 2011. Seasonal variation in marine C:N:P stoichiometry: can the composition of seston explain stable Redfield ratios? *Biogeosciences*, *8*(10), 2917–2933. DOI: https://doi.org/10.5194/bg-8-2917-2011

Froján, M., Figueiras, F. G., Zúñiga, D., Alonso-Pérez, F., Arbones, B. & Castro, C. G. 2016. Influence of Mussel Culture on the Vertical Export of Phytoplankton Carbon in a Coastal Upwelling Embayment (Ría de Vigo, NW Iberia). *Estuaries and Coasts*, *39*(5), 1449–1462. DOI: https://doi.org/10.1007/s12237-016-0093-1

Furlong, E. T. & Carpenter, R. 1988. Pigment preservation and remineralization in oxic coastal marine sediments. *Geochimica et Cosmochimica Acta*, *52*(1), 87–99. DOI: https://doi.org/10.1016/0016-7037(88)90058-0

Gardner, W. D., Biscaye, P. E. & Richardson, J. M. 1997. A sediment trap experiment in the Vema Channel to evaluate the effect of horizontal particle fluxes on measured vertical fluxes. *Journal of Marine Research*, *55*, 995–1028.

Garnier, J., Beusen, A., Thieu, V., Billen, G. & Bouwman, L. 2010. N:P:Si nutrient export ratios and ecological consequences in coastal seas evaluated by the ICEP approach. *Global Biogeochemical Cycles*, *24*(4). DOI: https://doi.org/10.1029/2009gb003583

Giannini, P. C. F., Guedes, C. C. F., Nascimento Jr, D. R. do, Tanaka, A. P. B., Angulo, R. J., Souza, M. C. de & Assine, M. L. 2009. Sedimentology and Morphological Evolution of the Ilha Comprida Barrier System, Southern São Paulo Coast. *In*: Dillenburg, S. R. & Hesp, P. A. (eds.), *Geology and Geomorphology of Holocene Coastal Barriers of Brazil* (pp. 177–224). Berlin: Springer.

Giovanardi, F. & Vollenweider, R. A. 2004. Trophic conditions of marine coastal waters: experience in applying the Trophic Index TRIX to two areas of the Adriatic and Tyrrhenian seas. *Journal of Limnology*, *63*(2), 199–218. DOI: https://doi.org/10.4081/jlimnol.2004.199

Grashoff, K.; Kremling. K. & Ehrhardt. M. 1983. Methods of seawater analysis. 2ed. Florida: Verlagie Chemie. 419p.

Groß, E., Pane, J. D., Boersma, M. & Meunier, C. L. 2022. River discharge-related nutrient effects on North Sea coastal and offshore phytoplankton communities. *Journal of Plankton Research*, *44*(6), 947–960. DOI: https://doi.org/10.1093/plankt/fbac049

Hamilton, S. K., Sippel, S. J. & Bunn, S. E. 2005. Separation of algae from detritus for stable isotope or ecological stoichiometry studies using density fractionation in colloidal silica. *Limnology and Oceanography: Methods*, *3*(3), 149–157. DOI: https://doi.org/10.4319/lom.2005.3.149

Hao, Y.-Y., Zhu, Z.-Y., Fang, F.-T., Novak, T., Čanković, M., Hrustić, E., Ljubešić, Z., Li, M., Du, J.-Z., Zhang, R.-F. & Gašparović, B. 2021. Tracing Nutrients and Organic Matter Changes in Eutrophic Wenchang (China) and Oligotrophic Krka (Croatia) Estuaries: A Comparative Study. *Frontiers in Marine Science*, *8*. DOI: https://doi.org/10.3389/fmars.2021.663601

Harari, J., França, C. A. S. & Camargo, R. 2008. Perspectives on Integrated Coastal Zone Management in South America. *In*: Neves, R., Baretta, J., Mateus, M. (ed.) *Climatology and hydrography of Santos Estuary* (pp. 147–160). Lisboa: IST Press.

Head, E. J. H. & Harris, L. R. 1996. Chlorophyll destruction by *Calanus* spp. grazing onphytoplankton: kinetics, effects of ingestion rate andfeeding history, and a mechanistic interpretation. *Marine Ecology Progress Series*, *135*, 223–235.

Ho, T.-Y., Quigg, A., Finkel, Z. V., Milligan, A. J., Wyman, K., Falkowski, P. G. & Morel, F. M. M. 2003. The elemental composition od some marine phytoplankton. *Journal of Phycology*, *39*(6), 1145–1159. DOI: https://doi.org/10.1111/j.0022-3646.2003.03-090.x

Honjo, S., Manganini, S. J., Krishfield, R. A. & Francois, R. 2008. Particulate organic carbon fluxes to the ocean interior and factors controlling the biological pump: A synthesis of global sediment trap programs since 1983. *Progress in Oceanography*, *76*(3), 217–285. DOI: https://doi.org/10.1016/j.pocean.2007.11.003

Hopkins, J., Henson, S. A., Poulton, A. J. & Balch, W. M. 2019. Regional Characteristics of the Temporal Variability in the Global Particulate Inorganic Carbon Inventory. *Global Biogeochemical Cycles*, *33*(11), 1328–1338. DOI: https://doi.org/10.1029/2019gb006300

Huang, J., Wang, S., Li, X., Xie, R., Sun, J., Shi, B., Liu, F., Cai, H., Yang, Q. & Zheng, Z. 2022. Effects of Shear Stress and Salinity Stratification on Floc Size Distribution During the Dry Season in the Modaomen Estuary of the Pearl River. *Frontiers in Marine Science*, *9*. DOI: https://doi.org/10.3389/fmars.2022.836927

Humborg, C., Smedberg, E., Medina, M. R. & Mörth, C.-M. 2008. Changes in dissolved silicate loads to the Baltic Sea — The effects of lakes and reservoirs. *Journal of Marine Systems*, *73*(3–4), 223–235. DOI: https://doi.org/10.1016/j.jmarsys.2007.10.014

INMET. 2020. Portal INMET. Accessed: http://www.inmet.gov.br/portal

IO-USP. 2006. MAPTOLAB. Accessed: http://www.mares.io.usp.br/

Italiani, D., Siegle, E. & Noernberg, M. A. 2020. Tidal inlet migration and formation: the case of the Ararapira inlet - Brazil. *Ocean and Coastal Research*, *68*. DOI: https://doi.org/10.1590/s2675-28242020068314

Jeffrey, S. W. & Humphrey, G. F. 1975. New spectrophotometric equations for determining chlorophylls a, b, c1 and c2 in higher plants, algae and natural phytoplankton. *Biochemie Und Physiologie Der Pflanzen*, *167*(2), 191–194. DOI: https://doi.org/10.1016/s0015-3796(17)30778-3

Joesoef, A., Huang, W.-J., Gao, Y. & Cai, W.-J. 2015. Air–water fluxes and sources of carbon dioxide in the Delaware Estuary: spatial and seasonal variability. *Biogeosciences*, *12*(20), 6085–6101. DOI: https://doi.org/10.5194/bg-12-6085-2015

Johannessen, S. C., O'Brien, M. C., Denman, K. L. & Macdonald, R. W. 2005. Seasonal and spatial variations in the source and transport of sinking particles in the Strait of Georgia, British Columbia, Canada. *Marine Geology*, *216*(1–2), 59–77. DOI: https://doi.org/10.1016/j.margeo.2005.01.004

John, D. M. 2003. Filamentous and Plantlike Green Algae. *In*: Wehr, J. D., Sheath, R. G., & Kociolek, J. P. (eds.), *Aquatic Ecology, Freshwater Algae of North America* (pp. 375–427). Elsevier. DOI: https://doi.org/10.1016/b978-0-12-385876-4.00008-6

Kähler, P. & Bauerfeind, E. 2001. Organic particles in a shallow sediment trap: Substantial loss to the dissolved phase. *Limnology and Oceanography*, *46*(3), 719–723. DOI: https://doi.org/10.4319/lo.2001.46.3.0719

Karlusich, J. J. P., Ibarbalz, F. M. & Bowler, C. 2020. Phytoplankton in the *Tara* Ocean. *Annual Review of Marine Science*, *12*(1), 233–265. DOI: https://doi.org/10.1146/annurev-marine-010419-010706

Kathiresan, K. 2003. How do mangrove forests induce sedimentation? *Revista de Biología Tropical*, *51*(2), 355–359.

Kostadinov, T. S., Siegel, D. A., Maritorena, S. & Guillocheau, N. 2012. Optical assessment of particle size and composition in the Santa Barbara Channel, California. *Applied Optics*, *51*(16), 3171–3189. DOI: https://doi.org/10.1364/ao.51.003171

Kutner, M. B. B. 1972. *Variação estacional e distribuição do fitoplâncton na região de Cananéia* (phdthesis). Universidade de São Paulo, Instituto Oceanográfico, São Paulo.

Lopes, R. M., Vale, R. do & Brandini, F. P. 1998. Composição, abundância e distribuição espacial do zooplâncton no complexo estuarino de Paranaguá durante o inverno de 1993 e o verão de 1994. *Revista Brasileira de Oceanografia*, *46*(2), 195–211. DOI: https://doi.org/10.1590/s1413-77391998000200008

Louda, J. W., Liu, L. & Baker, E. W. 2002. Senescence- and death-related alteration of chlorophylls and carotenoids in marine phytoplankton. *Organic Geochemistry*, *33*(12), 1635–1653. DOI: https://doi.org/10.1016/s0146-6380(02)00106-7

Lorenzen, C. J. 1965. A note on the chlorophyll and phaeophytin content of the chlorophyll maximum. *Limnology and Oceanography*, 10, 482-483.

Mari, X., Torréton, J.-P., Trinh, C. B.-T., Bouvier, T., Thuoc, C. V., Lefebvre, J.-P. & Ouillon, S. 2012. Aggregation dynamics along a salinity gradient in the Bach Dang estuary, North Vietnam. *Estuarine, Coastal and Shelf Science*, *96*, 151–158. DOI: https://doi.org/10.1016/j.ecss.2011.10.028

Martiny, A. C., Pham, C. T. A., Primeau, F. W., Vrugt, J. A., Moore, J. K., Levin, S. A. & Lomas, M. W. 2013. Strong latitudinal patterns in the elemental ratios of marine plankton and organic matter. *Nature Geoscience*, *6*(4), 279–283. DOI: https://doi.org/10.1038/ngeo1757

Mesquita, H. de S. L. & Peres, C. de A. 1985. Numerical contribution of phytoplanktonic cells, heterotrophic particles and bacteria to size fractionated POC in the Cananéia estuary (25°S 48°W), Brazil. *Boletim Do Instituto Oceanográfico*, *33*(1), 69–78.

Millo, C., Bravo, C., Covelli, S., Pavoni, E., Petranich, E., Contin, M., Nobili, M. D., Crosera, M., Sutti, B. O., Silva, C. das M. & Braga, E. de S. 2021. Metal Binding and Sources of Humic Substances in Recent Sediments from the Cananéia-Iguape Estuarine-Lagoon Complex (South-Eastern Brazil). *Applied Sciences*, *11*(18), 8466. DOI: https://doi.org/10.3390/app11188466

Miranda, L. B. de & Castro Filho, B. M. de. 1996. On the salt transport in the Cananéia sea during a spring tide experiment. *Revista Brasileira de Oceanografia*, *44*(2), 123–133.

Miyao, S. Y. & Harari, J. 1989. Estudo preliminar da maré e das correntes de maré da região estuarina de Cananéia (25°S-48°W). *Boletim Do Instituto Oceanográfico*, *37*(2), 107–123.

Miyao, S. Y., Nishihara, L. & Sarti, C. C. 1986. Características físicas e químicas do Sistema Estuarino-Lagunar de Cananéia-Iguape. *Boletim Do Instituto Oceanográfico*, *34*, 23–36.

Moraes, P. C., Zilius, M., Benelli, S. & Bartoli, M. 2018. Nitrification and denitrification in estuarine sediments with tube-dwelling benthic animals. *Hydrobiologia*, *819*(1), 217–230. DOI: https://doi.org/10.1007/s10750-018-3639-3

Moser, G. A. O., Gianesella, S. M. F., Alba, J. J. B., Bérgamo, A. L., Saldanha-Corrêa, F. M. P., Miranda, L. B. de & Harari, J. 2005. Instantaneous transport of salt, nutrients, suspended matter and chlorophyll-*a* in the tropical estuarine system of Santos. *Brazilian Journal of Oceanography*, *53*(3/4), 115–127.

Mostofa, K. M. G., Liu, C., Pan, X., Vione, D., Hayakawa, K., Yoshioka, T. & Komissarov, G. G. 2013. Chlorophylls and their Degradation in Nature. *In*: Mostofa, K. M. G., Yoshioka, T., Mottaleb, A., & Vione, D. (eds.), *Photobiogeochemistry of Organic Matter* (pp. 687–768). Berlin: Springer Berlin Heidelberg. DOI: https://doi.org/10.1007/978-3-642-32223-5_8

Nunes, L. H. 1990. *Impacto pluvial na serra do paranapiacaba e baixada santista* (phdthesis). Universidade de São Paulo, São Paulo.

Odebrecht, C., Villac, M. C., Abreu, P. C., Haraguchi, L., Gomes, P. D. F. & Tenenbaum, D. R. 2018. Flagellates Versus Diatoms: Phytoplankton Trends in Tropical and Subtropical Estuarine-Coastal Ecosystems. *In*: Hoffmeyer, M., Sabatini, M., Brandini, F., Calliari, D. & Santinelli, N. (eds.), *Plankton Ecology of the Southwestern Atlantic* (pp. 249–267). Springer International Publishing. DOI: https://doi.org/10.1007/978-3-319-77869-3_12

Pandolfini, E. 2000. Grazing experiments with two freshwater zooplankters: fate of chlorophyll and carotenoid pigments. *Journal of Plankton Research*, *22*(2), 305–319. DOI: https://doi.org/10.1093/plankt/22.2.305

Passow, U., Shipe, R. F., Murray, A., Pak, D. K., Brzezinski, M. A. & Alldredge, A. L. 2001. The origin of transparent exopolymer particles (TEP) and their role in the sedimentation of particulate matter. *Continental Shelf Research*, *21*(4), 327–346. DOI: https://doi.org/10.1016/s0278-4343(00)00101-1

Paula Filho, F. J., Marins, R. V., Chicharo, L., Souza, R. B., Santos, G. V. & Braz, E. M. A. 2020. Evaluation of water quality and trophic state in the Parnaíba River Delta, northeast Brazil. *Regional Studies in Marine Science*, *34*, 101025. DOI: https://doi.org/10.1016/j.rsma.2019.101025

Pilskaln, C. H., Padua, J. B., Chavez, F. P., Anderson, R. Y. & Berelson, W. M. 1996. Carbon export and regeneration in the coastal upwellingsystem of Monterey Bay, central California. *Journal of Marine Research*, *54*, 1149–1178.

Prado, H. M., Schlindwein, M. N., Murrieta, R. S. S., Júnior, D. R. do N., Souza, E. P. de, Cunha-Lignon, M., Mahiques, M. M. de, Giannini, P. C. F. & Contente, R. F. 2019. The Valo Grande Channel in theCananéia-Iguape Estuary-Lagoon Complex (SP, Brazil): Environmental

History, Ecology, and Future Perspectives. *Ambiente & Sociedade*, *22*. DOI: https://doi.org/10.1590/1809-4422asoc0182r2vu19l4td

Primpas, I. & Karydis, M. 2010. Scaling the trophic index (TRIX) in oligotrophic marine environments. *Environmental Monitoring and Assessment*, *178*(1–4), 257–269. DOI: https://doi.org/10.1007/s10661-010-1687-x

Raimonet, M., Thieu, V., Silvestre, M., Oudin, L., Rabouille, C., Vautard, R. & Garnier, J. 2018. Landward Perspective of Coastal Eutrophication Potential Under Future Climate Change: The Seine River Case (France). *Frontiers in Marine Science*, *5*. DOI: https://doi.org/10.3389/fmars.2018.00136

RAMSAR. 2017. Ramsar Sites Information Service. Accessed: https://rsis.ramsar.org/ris/2310

Rassmann, J., Lansard, B., Pozzato, L. & Rabouille, C. 2016. Carbonate chemistry in sediment porewaters of the Rhône River delta driven by early diagenesis (northwestern Mediterranean). *Biogeosciences*, *13*(18), 5379–5394. DOI: https://doi.org/10.5194/bg-13-5379-2016

Redfield, A. C. 1958. The biological control of chemical factors in the environment. *American Scientist*, *46*(3), 205–221.

Redfield, A. C., Ketchum, B. H. & Richards, F. A. 1963. The sea: ideas and observations on progress in the study of the seas. *In*: Hill, M. N. (ed.) *The Sea.* (2nd ed., pp. 26–77). New York: Wiley.

Regnier, P., Friedlingstein, P., Ciais, P., Mackenzie, F. T., Gruber, N., Janssens, I. A., Laruelle, G. G., Lauerwald, R., Luyssaert, S., Andersson, A. J., Arndt, S., Arnosti, C., Borges, A. V., Dale, A. W., Gallego-Sala, A., Goddéris, Y., Goossens, N., Hartmann, J., Heinze, C., Ilyina, T., Joos, F., LaRowe, D. E., Leifeld, J., Meysman, F. J. R., Munhoven, G., Raymond, P. A., Spahni, R., Suntharalingam, P. & Thullner, M. 2013. Anthropogenic perturbation of the carbon fluxes from land to ocean. *Nature Geoscience*, *6*(8), 597–607. DOI: https://doi.org/10.1038/ngeo1830

Saavedra-Hortua, D. A., Friess, D. A., Zimmer, M. & Gillis, L. G. 2020. Sources of Particulate Organic Matter across Mangrove Forests and Adjacent Ecosystems in Different Geomorphic Settings. *Wetlands*, *40*(5), 1047–1059. DOI: https://doi.org/10.1007/s13157-019-01261-9

Saderne, V., Geraldi, N. R., Macreadie, P. I., Maher, D. T., Middelburg, J. J., Serrano, O., Almahasheer, H., Arias-Ortiz, A., Cusack, M., Eyre, B. D., Fourqurean, J. W., Kennedy, H., Krause-Jensen, D., Kuwae, T., Lavery, P. S., Lovelock, C. E., Marba, N., Masqué, P., Mateo, M. A., Mazarrasa, I., McGlathery, K. J., Oreska, M. P. J., Sanders, C. J., Santos, I. R., Smoak, J. M., Tanaya, T., Watanabe, K. & Duarte, C. M. 2019. Role of carbonate burial in Blue Carbon budgets. *Nature Communications*, *10*(1), 1106. DOI: https://doi.org/10.1038/s41467-019-08842-6

Sanders, T. & Laanbroek, H. J. 2018. The distribution of sediment and water column nitrification potential in the hyper-turbid Ems estuary. *Aquatic Sciences*, *80*(4). DOI: https://doi.org/10.1007/s00027-018-0584-1

Santos, A. K. D. dos S., Cutrim, M. V. J., Costa, D. S., Cavalcanti, L. F., Ferreira, F. S., Oliveira, A. L. L. & Serejo, J. H. F. 2021. Algal blooms and trophic state in a tropical estuary blocked by a dam (northeastern Brazil). *Ocean and Coastal Research*, *69*, 21009. DOI: https://doi.org/10.1590/2675-2824069.20-006akddss

Santos, A. L. dos, Gourvil, P., Tragin, M., Noël, M.-H., Decelle, J., Romac, S. & Vaulot, D. 2016. Diversity and oceanic distribution of prasinophytes clade VII, the dominant group of green algae in oceanic waters. *The ISME Journal*, *11*(2), 512–528. DOI: https://doi.org/10.1038/ismej.2016.120

Sarma, V. V. S. S., Arya, J., Subbaiah, C. V., Naidu, S. A., Gawade, L., Kumar, P. P. & Reddy, N. P. C. 2012. Stable isotopes of carbon and nitrogen in suspended matter and sediments from the Godavari estuary. *Journal of Oceanography*, *68*(2), 307–319. DOI: https://doi.org/10.1007/s10872-012-0100-5

Schagerl, M., Pichler, C. & Donabaum, K. 2003. Patterns of major photosynthetic pigments in freshwater algae. 2. Dinophyta, Euglenophyta, Chlorophyceae and Charales. *Annales de Limnologie - International Journal of Limnology*, *39*(1), 49–62. DOI: https://doi.org/10.1051/limn/2003005

Schulz, G., Sanders, T., Beusekom, J. E. E. van, Voynova, Y. G., Schöl, A. & Dähnke, K. 2022. Suspended particulate matter drives the spatial segregation of nitrogen turnover along the hyper-turbid Ems estuary. *Biogeosciences*, *19*(7), 2007–2024. DOI: https://doi.org/10.5194/bg-19-2007-2022

Sharoni, S. & Halevy, I. 2020. Nutrient ratios in marine particulate organic matter are predicted by the population structure of well-adapted phytoplankton. *Science Advances*, *6*(29). DOI: https://doi.org/10.1126/sciadv.aaw9371

Silva, I. F. 1989. Dados climatológicos de Cananéia e Ubatuba (Estado de São Paulo). Série de 1956-1985. *Boletim Climatológicodo Instituto Oceanográfico*, *6*, 1–21.

Sutti, B. O., Guimarães, L. L. & Borges, E. S. 2022. River Flows Influence on Nutrients (Si, N and P) and Fecal Coliforms (E. coli) in Two Tributaries of the Estuarine Channel of Bertioga (Santos Estuary, São Paulo, Brazil). *Journal of Geoscience and Environment Protection*, 10, 26-46.

Sutti, B. O., Guimarães, L. L., Borges, R. P. & Schmiegelow, J. M. M. 2015. Avaliação do silicato dissolvido como sinalizador de processos erosivos nabacia de drenagem de sistemas estuarinos. *UNISANTA BioScience*, *4*(2), 105–110.

Thill, A., Moustier, S., Garnier, J.-M., Estournel, C., Naudin, J.-J. & Bottero, J.-Y. 2001. Evolution of particle size and concentration in the Rhône river mixing zone: influence of salt flocculation. *Continental Shelf Research*, 21 (18–19), 2127–2140. DOI: https://doi.org/10.1016/s0278-4343(01)00047-4

Tréguer, P. & Le Corre, P. 1975. *Manuel d'analyse des sels nutritifs dans l'eau de mer* (2nd ed.). Brest: Université de Bretage Occidentale.

Tundisi, J. G. & Matsumura-Tundisi, T. 2001. Coastal Marine Ecosystems of Latin America. *In*: Seeliger, U. & Kjerfve, B. (eds.), *Ecological Studies* (pp. 119–130). Berlin: Springer Berlin Heidelberg. DOI: https://doi.org/10.1007/978-3-662-04482-7_10

Turner, J. T. 2015. Zooplankton fecal pellets, marine snow, phytodetritus and the ocean's biological pump. *Progress in Oceanography*, *130*, 205–248. DOI: https://doi.org/10.1016/j.pocean.2014.08.005

Turner, R. E., Qureshi, N., Rabalais, N. N., Dortch, Q., Justic, D., Shaw, R. F. & Cope, J. 1998. Fluctuating silicate:nitrate ratios and coastal plankton food webs. *Proceedings of the National Academy of Sciences*, *95*(22), 13048–13051. DOI: https://doi.org/10.1073/pnas.95.22.13048

UNESCO. 1999. *Decision of the world heritage committee* (resreport No. 23 Session of the World Heritage). Geneva: UNESCO.

Verney, R., Lafite, R. & Brun-Cottan, J.-C. 2009. Flocculation Potential of Estuarine Particles: The Importance of Environmental Factors and of the Spatial and Seasonal Variability of Suspended Particulate Matter. *Estuaries and Coasts*, *32*(4), 678–693. DOI: https://doi.org/10.1007/s12237-009-9160-1

Wang, A., Liu, J. T., Ye, X., Zheng, B., Li, Y. & Chen, J. 2015. Settling fluxes of cohesive sediments measured by sediment traps in a semi-enclosed embayment with strong tidal environments. *Continental Shelf Research*, *106*, 17–26. DOI: https://doi.org/10.1016/j.csr.2015.04.026

Yacobi, Y. Z. & Ostrovsky, I. 2008. Downward flux of organic matter and pigments in Lake Kinneret (Israel): relationships between phytoplankton and the material collected in sediment traps. *Journal of Plankton Research*, *30*(10), 1189–1202. DOI: https://doi.org/10.1093/plankt/fbn070

Yadav, A. & Pandey, J. 2018. The pattern of N/P/Si stoichiometry and ecological nutrient limitation in Ganga River: up- and downstream urban influences. *Applied Water Science*, *8*(3), 94. DOI: https://doi.org/10.1007/s13201-018-0734-6

Yao, Y., Liu, H., Han, R., Li, D. & Zhang, L. 2021. Identifying the Mechanisms behind the Positive Feedback Loop between Nitrogen Cycling and Algal Blooms in a Shallow Eutrophic Lake. *Water*, *13*(4), 524. DOI: https://doi.org/10.3390/w13040524

Zajączkowski, M. 2002. On the use of sediment traps in sedimentationmeasurements in glaciated fjords. *Polish Polar Research*, *23*(2), 161–174.

Zhang, P., Peng, C.-H., Zhang, J.-B., Zou, Z.-B., Shi, Y.-Z., Zhao, L.-R. & Zhao, H. 2020. Spatiotemporal Urea Distribution, Sources, and Indication of DON Bioavailability in Zhanjiang Bay, China. *Water*, *12*(3), 633. DOI: https://doi.org/10.3390/w12030633

Zhang, X., Stavn, R. H., Falster, A. U., Gray, D. & Gould, R. W. 2014. New insight into particulate mineral and organic matter in coastal ocean waters through optical inversion. *Estuarine, Coastal and Shelf Science*, *149*, 1–12. DOI: https://doi.org/10.1016/j.ecss.2014.06.003

Zhu, W., Wang, C., Hill, J., He, Y., Tao, B., Mao, Z. & Wu, W. 2018. A missing link in the estuarine nitrogen cycle?: Coupled nitrification-denitrification mediated by suspended particulate matter. *Scientific Reports*, *8*(1), 2282. DOI: https://doi.org/10.1038/s41598-018-20688-4

Zilli, M. T., Carvalho, L. M. V., Liebmann, B. & Dias, M. A. S. 2016. A comprehensive analysis of trends in extreme precipitation over southeastern coast of Brazil. *International Journal of Climatology*, *37*(5), 2269–2279. DOI: https://doi.org/10.1002/joc.4840

Zúñiga, D., Villacieros-Robineau, N., Salgueiro, E., Alonso-Pérez, F., Rosón, G., Abrantes, F. & Castro, C. G. 2016. Particle fluxes in the NW Iberian coastal upwelling system: Hydrodynamical and biological control. *Continental Shelf Research,* 123, 89-98.